Chapter 2

Design and Analysis of 64 × 64 Silicon-on-Insulator Arrayed Waveguide Grating Planner Optical Waveguide Device

In this chapter, we use the beam propagation method (BPM) to simulate the transmission characteristics of a 64×64-channel arrayed waveguide grating multi/demultiplexer with a channel spacing of 50GHz. The AWG has a channel spacing of 0.4 nm with its spectrum centered at 1550.52 nm. In the phase array section, the number of arrayed waveguides is 266 and the length difference is 9.89 μm. We present the design, simulation and performance of a 64×64-channel arrayed waveguide grating demultiplexer with SOI photonic integrated circuit technology in the following sections. This chapter is arranged as follows: Section 2-1 introduces basics of the AWG and of SOI waveguide. The advantages of AWG applied in wavelength division multiplexing fiber-optic communication system are presented and discussed. We also present the theory and fundamental characteristics and design process of AWG in Section 2-2 and 2-3. Section 2-4 describes the simulation result of a 64×64-channel AWG in the silicon-on-insulator structure is made of the “WDM_Phasar” package from the Optiwave Corporation, which uses the Fast Fourier Transform Beam Propagation Method to simulate light wave propagation in optical waveguides are presented. The fundamental mode is used as our initial mode to simulate the propagation condition for 64×64-channel arrayed waveguide grating based on the simulator WDM_PHASER. We also give the summary and discussions of our designed 64×64-channel AWG in the final section 2-5.

2-1 Introduction of the basics of Arrayed Waveguide Grating

Recently, the device developments of the WDM components and systems for optical communications are rapidly increased [28]. The WDM technique provides benefits for increasing capacity and network design flexibility in the telecommunication networks. The arrayed waveguide grating (AWG) technologies have attracted lots of attentions recently [29-30]. AWG multiplexes / demultiplexes [31-32] with low insertion loss and high stability are the most promising devices for application consideration in WDM backplane interconnection systems. Especially, AWGs are important building blocks in the development of multiple channel integrated devices for routing and channel add-drop in dense wavelength division multiplexing (DWDM) interconnection systems [33-35].

The demand of bandwidth in optical interconnections is rapidly increasing. Therefore, WDM components are becoming more important for solving capacity and flexibility problems in the optical interconnection network. The wavelength multiplexers and demultiplexers is one of the key components in WDM systems. As well as performing basic multiplexing and demultiplexing functions, they can be combined with other components to create add/drop multiplexers. These devices can be passive, where the signal routing is fixed according to wavelength, or active, where optical switches are utilised to dynamically route the signals. Both circuits shown are transparent to the data format, can allow bidirectional transfer of information, and function entirely in the optical domain. Many principles have been proposed and reported. Before research on (de)multiplexers has been increasing focus on AWG, they are known under different names: Dragone-Smit router, Phased Arrays (PHASARs) [36-40], Waveguide Grating Router (WGRs) and Array Waveguide Gratings (AWGs). The AWG plays a crucial role in the realization of modern optical networks. The AWG will be presented about introducing the principles of operation of the AWG, and then examines the design process in the following sections. In this paper we focus on multi-port by multi-port AWG, it may look like conventional one port by multi-port AWG-based (de)multiplexers where the input and output ports has been increased. The multi-port by multi-port AWG is capable of processing multi-port by multi-port optical interconnection in a strictly nonblocking way due to the cyclic rotation property of the output wavelength. The development of optical and optoelectronic devices in silicon-on-insulator (SOI) [41-44] offers a path toward low-cost, monolithic multi-wavelength optical receiver system including the wavelength demultiplexer, photodetectors, and electronic circuits.

2-2 64×64 Arrayed Waveguide Grating Principles

2-2-1 Single Mode Rib Waveguide

Single mode propagation is an important requirement in optical devices. It was first reported by Peterman [45] in 1976, he uses Mode-matching and BPM to analyze semiconductor rib waveguide and then apply to silicon rib waveguide. Equation (2-1) and (2-2) give the condition to design a single-mode waveguide for SOI structure.

$$\frac{W}{H} \le \alpha + \frac{\frac{h}{H}}{\sqrt{1-\left(\frac{h}{H}\right)^2}} \qquad (2-1)$$

$$\frac{h}{H} \ge 0.5 \qquad (2-2)$$

As shown in Fig. 2-1, the single mode rib waveguide of 64×64 AWG with the width of rib waveguide W = 5.3μm. h = 5μm is the height of slab waveguide and H = 6.7μm is the total rib height. α = 0.3 is a dimensionless constant. We adopt channel waveguides structure for achieving AWG. The refractive index of the channel waveguide is 3.45 and the cladding layer is controlled at 1.48 through the photolithography process. The AWG is designed by the single mode formula as shown in equation (2-1) and equation (2-2). The mode pattern of the single rib waveguide is shown in Fig. 2-2.

2-2-2 Theoretical Model of an Arrayed Waveguide Grating

When the light propagates from input port waveguide then enters the free propagation region (FPR), it becomes divergent. On arriving at the input port of the phase array, the beam coupled into the waveguide array and propagate through the individual waveguide array. The adjacent array waveguide has equal path length difference. The output aperture is equal for this wavelength of the individual phase array waveguide, so the field and phase at input waveguide array can be reproduced at the FPR on the opposite side of the array. Fig. 2-7 gives the enlarge view of the FPR I, d_I is input waveguide separation, d_{PAI} is the spacing of the arrayed waveguide at the input end that follows a curvature with a radius of f_{FPRI}, and the distance measured in clockwise direction from the center input is x_I, which corresponds to an angular distance θ_I. The geometrical structure of the FPR I is given by the Rowland circle construction, the input waveguide is displaced at the input focal curve and the radius of curvature of the input focal curve is half the radius of curvature of the interface between FPR I and the waveguide array.

In the output slab region, the same construction applies for the FPR II, d_{II} is the output waveguide spacing, d_{PAII} is the spacing of the arrayed waveguide at the output end that follows a curvature with a radius of f_{FPRII}, and the distance measured in clockwise direction from the center output is x_{II}, which corresponds to an angular distance θ_{II}. We consider the phase delays of the k-th and *(k-1)*-th arrayed waveguide, two light beam passing through must be an integral multiple of 2π, based on the interference condition as [46-47]

$$\beta_s(\lambda_c)\left(f_{FPRI}-\frac{d_{PAI}}{2}\sin\theta_I\right)+\beta_c(\lambda_c)\left[L_o+(k-1)\Delta L\right]+\beta_s(\lambda_c)\left(f_{FPRII}+\frac{d_{PAII}}{2}\sin\theta_{II}\right)=$$
$$\beta_s(\lambda_c)\left(f_{FPRI}+\frac{d_{PAI}}{2}\sin\theta_I\right)+\beta_c(\lambda_c)\left[L_o+k\Delta L\right]+\beta_s(\lambda_c)\left(f_{FPRII}-\frac{d_{PAII}}{2}\sin\theta_{II}\right)-2m\pi$$

(2-3)

Where β_s and β_c donate the propagation constants in slab region and arrayed waveguide, λ_c is the center wavelength, and L_o is the minimum arrayed waveguide length, m is an integral. From the definitions, the following equations are obvious

$$\theta_I = x_I / f_{FPRI} = i \bullet \Delta x_I / f_{FPRI} \qquad \theta_{II} = x_{II} / f_{FPRII} = j \bullet \Delta x_{II} / f_{FPRII} \qquad (2\text{-}4)$$

Substituting equation (2-4) into equation (2-3), we get

$$\beta_s(\lambda_c)\left(f_{FPRI}-\frac{d_{PAI}x_I}{2f_{FPRI}}\right)+\beta_c(\lambda_c)[L_o+(k-1)\Delta L]+\beta_s(\lambda_c)\left(f_{FPRII}+\frac{d_{PAII}x_{II}}{2f_{FPRII}}\right)=$$
$$\beta_s(\lambda_c)\left(f_{FPRI}+\frac{d_{PAI}x_I}{2f_{FPRI}}\right)+\beta_c(\lambda_c)[L_o+k\Delta L]+\beta_s(\lambda_c)\left(f_{FPRII}-\frac{d_{PAII}x_{II}}{2f_{FPRII}}\right)-2m\pi$$

(2-5)

Subtracting common terms, and because of our discussion of the symmetrical Arrayed Waveguide Grating, hence, $\sin\theta_I = \sin\theta_{II}$, and $f_{FPRI} = f_{FPRII}$, here obtain

$$\beta_s(\lambda_c)\left(\frac{d_{PAI}x_I}{f_{FPRI}}\right)-\beta_s(\lambda_c)\left(\frac{d_{PAII}x_{II}}{f_{FPRII}}\right)+\beta_c(\lambda_c)\Delta L=2m\pi \quad (2\text{-}6)$$

Under the condition $\beta_c(\lambda_c)\Delta L = 2m\pi$ or $\lambda_c = \frac{n_{PAW}\Delta L}{m}$ (2-7)

where n_{PAW} is the effective refractive index of the arrayed waveguide and m is called as a diffraction order ($n_{PAW}=\beta_c/k$, k is the wave number in vacuum). The light input position x_I and output position x_{II} satisfy the following equation:

$$\frac{d_{PAI}x_I}{f_{FPRI}}=\frac{d_{PAII}x_{II}}{f_{FPRII}} \quad (2\text{-}8)$$

the dispersion of the output focal position x_{II} with respect to the wavelength for the fixed input position x_I is obtained by differentiating equation (2-6) with respect to wavelength λ_c as

$$\frac{\Delta x_{II}}{\Delta\lambda}=\frac{n_g f_{FPRII}\Delta L}{n_{FPR} d_{PAII}\lambda_c} \qquad (2\text{-}9)$$

where n_{FPR} is the effective index of the Free Propagation Region, n_g is regarded as group index of the arrayed waveguide ($n_g = n_{PAW}-\lambda dn_{PAW}/d\lambda$) [48]. Similarly, the dispersion of the input position x_I with respect to the wavelength for the fixed output position x_{II} is also obtained with respect to wavelength λ as [46]

$$\frac{\Delta x_I}{\Delta\lambda}=\frac{n_g f_{FPRI}\Delta L}{n_{FPR} d_{PAI}\lambda_c} \qquad (2\text{-}10)$$

when $\Delta\lambda$ is set to the wavelength channel spacing, the Δx_I and Δx_{II} should be the input and output waveguide separations d_I and d_{II}, respectively. Symmetrical array waveguide grating, the input slab and output slab are identical, that is, $d_{PAI}=d_{PAII}=d_{PA}$, $d_I=d=d_{II}$, $f_{FPR}=f_{FPRI}=f_{FPRII}$. When the divergent beam of the input ports propagate at the output of the array waveguide in the FPR II, then we get

$$\Delta L=\frac{n_{FPR} d d_{PA}\lambda_c}{n_g f_{FPR}\Delta\lambda} \qquad (2\text{-}11)$$

The angular dispersion, which is the relation between diffraction angle θ and frequency f can be also obtained by combining equation (2-4) and (2-11):

$$\frac{d\theta}{df} = -\frac{m\lambda_c^2 n_g}{n_{FPR} d_{PA} c n_{PAW}} \tag{2-12}$$

The spatial separation of the m-th and (m+1)-th order focused beams for the same wavelength is obtained from equation (2-3) as

$$X_{FSR} = x_m - x_{m-1} = \frac{f_{FPR}\lambda_c}{n_{FPR} d_{PA}} \tag{2-13}$$

X_{FSR} is the free spatial range of the arrayed waveguide grating. Number of available wavelength maximum channels N_{ch} is thus determined by dividing X_{FSR} with the output waveguide separation d_{II} as

$$N_{ch} = \frac{X_{FSR}}{d_{II}} = \frac{f_{FPR}\lambda_C}{n_{FPR} d_{PA} d_{II}} \tag{2-14}$$

Equation (2-3) can also be written in another form as equation (2-15):

$$n_{FPR} d_I \sin\theta_I + n_{PAW}\Delta L + n_{FPR} d_{II} \sin\theta_{II} = m\lambda = m\frac{c}{f} \tag{2-15}$$

For the order of m+1, equation (2-15) is changed into equation (2-16) below:

$$(n_{FPR} + \Delta n_{FPR}) d_I \sin\theta_I + (n_{PAW} + \Delta n_{PAW})\Delta L + (n_{FPR} + \Delta n_{FPR}) d_{II} \sin\theta_{II} = (m+1)\frac{c}{f + FSR} \tag{2-16}$$

where $n_{FPR}+\Delta n_{FPR}$ and $n_{PAW}+\Delta n_{PAW}$ are the effective indices of the free propagation region and channel waveguides, respectively, at the frequency of f+FSR. The index change is approximated by

$$\Delta n_{PAW} = \frac{\partial n_{PAW}}{\partial f} FSR = -\frac{c}{f^2} \frac{\partial n_{PAW}}{\partial \lambda} FSR \tag{2-17}$$

$$\Delta n_{FPR} = \frac{\partial n_{FPR}}{\partial f} FSR = -\frac{c}{f^2} \frac{\partial n_{FPR}}{\partial \lambda} FSR \tag{2-18}$$

From Eq. (2-15) to (2-18), the FSR is given as

$$FSR = \frac{c}{\left(n_{PAW} - \lambda \frac{\partial n_{PAW}}{\partial \lambda} \right) \Delta L + \left(n_{FPR} - \lambda \frac{\partial n_{FPR}}{\partial \lambda} \right) \left(d_I \sin \theta_I + d_{II} \sin \theta_{II} \right)} \tag{2-19}$$

For

$$n_g \approx n_{PAW} - \lambda \frac{\partial n_{PAW}}{\partial \lambda} \approx n_{FPR} - \lambda \frac{\partial n_{FPR}}{\partial \lambda} \tag{2-20}$$

we get

$$FSR = \frac{c}{n_g \left(\Delta L + d_I \sin \theta_I + d_{II} \sin \theta_{II} \right)} \qquad [Hz] \tag{2-21}$$

and $\Delta L >> \left(d_I \sin \theta_I + d_{II} \sin \theta_{II} \right)$ (2-22)

we get the relation:

$$FSR = \frac{c}{n_g \Delta L} \qquad or \qquad \frac{\lambda n_{PAW}}{m n_g} \qquad [Hz] \tag{2-23}$$

It is apparent that different input-output route has different FSR.

Equation (2-14) can also be written in another form by equation (2-23) as equation (2-24):

$$N_{ch} = \frac{FSR}{\Delta f} = \frac{FSR}{\Delta\lambda} \tag{2-24}$$

Δf and $\Delta\lambda$ are the spacing of the frequency and the wavelength, respectively. In fact, in order to prevent optical field between diffraction progression producing overlap on the spectrum, so $N\Delta f$ must be smaller than FSR, we can be given as equation (2-25):

$$N_{ch} \leq \frac{FSR}{\Delta f} = \frac{c}{n_g \Delta L \Delta f} \qquad or \qquad N_{ch} \leq \frac{FSR}{\Delta\lambda} = \frac{c}{n_g \Delta L \Delta\lambda} \tag{2-25}$$

2-2-3 Operation of the 64×64 Arrayed Waveguide Grating

We established that AWGs are essential components for the knowledge of optical communication, networks and DWDM. In this section, the basic operation of a 64×64 AWG as a de-multiplexer is described.

Fig. 2-3 shows the top view of the 64×64 AWG. The input (a) consists of 64-channels, carried on separate frequencies. Channel spacings of 100GHz or 50 GHz are common in commercial devices, although 25GHz [49] and 10GHz [50] spacings have been achieved under laboratory conditions. The operational wavelength is commonly around 1.55μm where attenuation is lowest in optical fibers. All waveguides in the AWG tend to be single-mode to ensure predictable propagation through the device.

Light couples from the input waveguide (a) into the Free Propagation Region I (FPR I) (b) and disperses to illuminate the phased arrayed waveguides (PAWs) starting on a curved plane, along the light displays a constant phase profile. Each PAW increases in length by ΔL compared to the previous one in the array waveguides, where $\Delta L = m\lambda_c / n_{PAW}$, m is an integer number, λ_c is the central operational wavelength, and n_{PAW} is the effective refractive index, (β_c/k), of the single mode supported by each waveguide forming the AWG. Consequently, at the central wavelength, a constant phase profile is exhibited at the end of the PAWs, an integer number of cycles out of phase, along the same plane, as shown in Fig. 2-7. Therefore, at the central frequency, the light focuses at the center of the plane (e), where an output waveguide is positioned to capture the focussed light. Different wavelengths of light will display different amounts of phase change, due to the increments in length of each waveguides, the phases will change along the PAW output plane, causing the focal point to move along the focal plane (e) at the end of the Free Propagation Region II (FPR II). An output waveguide is positioned on the output plane to pick up each input channel (wavelength).

2-3 Design Methods of 64×64 Arrayed Waveguide Grating

2-3-1 Introduction

This section looks at the analytical methods to design an AWG. The design of an 64 × 64 AWG is covered in detail in [51-55]. An AWG is specified by the following characteristics:

- ✧ Number of Channels
- ✧ Central Wavelength, and Channel spacing
- ✧ Insertion loss
- ✧ Crosstalk level
- ✧ Uniformity

We concentrate on the basic design rules that govern AWG dimensions.

2-3-2 Definition of the High-Level Parameters of Arrayed Waveguide Gratings

For insertion loss in the AWG, the primary cause is due to inefficient coupling at the interface between the FPR I and the PAWs. Due to reciprocity [53], identical loss occurs at the PAW–FPR II interface into higher diffraction orders. Coupling influence, and insertion loss is largely determined by the separation of the PAWs at these interfaces, where smaller separations increase the coupling efficiency [53]. However, at small separations, coupling between the PAWs becomes significant. This effect has to be carefully quantified through the Beam Propagation Method (BPM) to avoid phasing errors in the PAWs. Other areas that cause loss may include

- Scattering due to fabrication errors and waveguide roughness
- De-focussing of the spot on the output plane due to phase errors, decreasing coupling efficiency into the output waveguide
- Material losses.

The excess loss of the arrayed waveguide grating is caused by inconsistencies in the field distribution of the arrayed waveguides and free propagation region. The total coupling efficiency, therefore, is given by [56]

$$\eta = \sum_{i}^{M} \left(\int f(x) g_i(x) dx \right)^2 \tag{2-26}$$

where $f(x)$ and $g_i(x)$ are the optical field distributions at the FPR-PAWs interface in the FPR and in the i-th waveguide array, respectively. The rib waveguide gives us a simple approximation [57], given by

$$\eta \approx \frac{8W}{\pi^2 (W + G)} \tag{2-27}$$

where W is the waveguide width and G is the gap between waveguides array.

Frequency response is an important transmission coefficient of AWG. Each light enters from input waveguide, coupled into FPR I then passing through the PAWs, focusing in the FPR II, and coupled into the output waveguide. The mode patterns of the focused light and propagation mode of the output waveguide are almost the same. Here, we analyze the frequency response with Gaussian mode. The coupling coefficient of the [58]

$$T(\Delta f) = \exp\left[-\left(\frac{L_{FPR}D}{w_p}\right)^2\right] \tag{2-28}$$

D is dispersion and w_p is the effective width of the modal field, and the Full Width at Half Maximum (FWHM) is given by [59]

$$FWHM = \frac{2\sqrt{\ln 2}\,w_p \Delta f}{\Delta x_j} \tag{2-29}$$

Channel spacing of the WDM signal is $\Delta\lambda$. To put these relations into (2-11), the wavelength spacing$\Delta\lambda$ for the fixed light input position is given by

$$\Delta\lambda = \frac{n_{FPR} d d_{PA} \lambda_o}{n_g L_{FPR} \Delta L} \tag{2-30}$$

The nonuniformity L_u is defined as the intensity ratio (in dB) between the central channel and the outermost channel. Using a Gaussian-beam approximation for the intensity of the far-field we can find the following dependence for the nonuniformity [60].

$$L_u = -10\log\left[\exp(-2\theta_{\max}^2/\theta_o^2)\right] \tag{2-31}$$

where θ_o is the width of the fundamental mode field of a single waveguide from the phase array

$$\theta_o = \frac{\lambda}{n_{FPR} w_p \sqrt{2\pi}} \tag{2-32}$$

where w_p is the effective width of the arrayed waveguide modal field given by the following expression

$$w_p = \frac{\int_{-\infty}^{+\infty} E(x)^2\,dx}{E_{\max}^2} \tag{2-33}$$

the angle corresponding to the outer channel can be found from

$$\theta_{\max} = \frac{S_{\max}}{D^{\min i}} \tag{2-34}$$

For channel crosstalk, the causes are many, and may be a result of the design or imperfect fabrication of the AWG. The primary source taken into account in initial design is the channel crosstalk, caused in the FPR II with adjacent output waveguides by the overlap of the focused spot [51].

Designs must be more rigorous take into account potential PAW phase error, caused by design or fabrication carelessness, which cause the spot to spread, increasing crosstalk. This crosstalk is easily controlled by increasing the separation of the output waveguides and adding tapered waveguide at the junction of input/output port and FPR.

2-3-3 Design of 64-Channel Arrayed Waveguide Grating

The 64 × 64 AWG includes the input/output ports, the star coupler and the phased arrayed waveguides. The schematic diagram of our designed 64×64 SOI AWG is shown in Fig. 2-3. The location of this focal position depends on the signal wavelength λ because the relative phase delay in each waveguide is given by $\Delta L/\lambda$. The path length difference ΔL is 9.89μm which is obtained by the calculation of equation (2-11) in our design. From the result of calculation of equation (2-9) and (2-10), the corresponding grating order at λ_C = 1.55μm is 22 which gives a dispersion of 13.6nm (107.4MHz). A free spectral range of 69.56 nm (8.9THz) is designed by using equation (2-23). This AWG is designed with a channel spacing of 0.4nm (50GHz) for DWDM applications. The bending radius varies from 2.5 to 6.3μm and the waveguide width of each waveguide of phase array is 5.3μm. The occupied area of the phased arrayed waveguide is 1.0×0.3cm^2 and the total device size is $8.32 \times 1.87 cm^2$.

In our designed AWG, it consists of 64 input/output waveguides, two focusing slab regions with arc length of 13.2mm and a phase array of 266 rib waveguides with the constant: path length difference between neighbouring waveguides. The input light is launched into the first input waveguide, and then the light goes through the arrayed waveguides. Finally, the light beams converge into the focal position in the second slab. Table II shows our calculated design parameters for 64×64 AWG MUX/DeMUX based on SOI substrate. After modeling the behavior of arrayed waveguide grating equation, some physical parameters should be set in order to comply the specifications in optical network, such as channel spacing, uniformity, insertion loss, and frequency bandwidth, as shown in Table III, are needed in order to properly design these devices.

2-4 Simulation Results and Analysis of 64╳64 Channel Arrayed Waveguide Grating

2-4-1 Beam Propagation Method Principles

Curvilineal directional couplers, branching and combining waveguides, S-shaped bent waveguides, and tapered waveguide are indispensable components in constructing integrated optical circuits. Mode coupling phenomena in parallel directional couplers have been investigated. In practical directional coupler, however, light coupling in the S-shaped bent waveguide regions in the front and rear of parallel waveguides should be taken into account so as to evaluate the propagation characteristics precisely. The beam propagation method (BPM) [61-63] is the most powerful technique to investigate linear and nonlinear lightwave propagation phenomena in axially varying waveguides such as curvilinear directional couplers, branching and combining waveguides, S-shaped bent waveguides, and tapered waveguides. BPM is also quite important for the analysis of ultrashort light pulse propagation in optical fibers.

Basic equations for beam propagation method based on Fourier transform.

The three-dimensional scalar wave equation (Helmholtz equation), which is the basis of BPM, is expressed by

$$\frac{\partial^2 E}{\partial x^2}+\frac{\partial^2 E}{\partial y^2}+\frac{\partial^2 E}{\partial y^2}+k_o^2 n^2(x,y,z)E=0 \tag{2-35}$$

We separate the electric field $E(x,y,z)$ into two parts: the axially slowly varying envelope term of $\phi(x,y,z)$ and the rapidly varying term of exp(*-jkn₀z*). Here, n_0 is a refractive index in the cladding. Then, $E(x,y,z)$ is expressed by

$$E(x,y,z)=\phi(x,y,z)e^{-jkn_0 z} \tag{2-36}$$

Substituting equation (2-36) into equation (2-35), we obtain

$$\nabla^2\phi - j2kn_0\frac{\partial\phi}{\partial z}+k^2\left(n^2-n_0^2\right)=0 \tag{2-37}$$

Where

$$\nabla^2=\frac{\partial^2}{\partial x^2}+\frac{\partial^2}{\partial y^2}+\frac{\partial^2}{\partial z^2} \tag{2-38}$$

Assuming the weakly guiding condition, we can approximate $\left(n^2-n_0^2\right)\cong 2n_0\left(n-n_0\right)$ in equation (2-37) can be rewritten as

$$\frac{\partial\phi}{\partial z}=-j\frac{1}{2kn_0}\nabla^2\phi - jk\left(n-n_0\right)\phi \tag{2-39}$$

Equation (2-39) is a basic formula for BPM simulations.

The disadvantages of the conventional BPM are that they only discussed the scalar wave equations [64-67]. However, the vectorial properties may be important and even essential if the polarization is of concern. Therefore, it is necessary to model and simulate the vectorial electromagnetic wave propagating in the guided-wave devices. By recognizing the electric field E is a vector to calculate the polarization effect in the BPM. The derivation is from the vector wave equation rather than the scalar helmholtz equation [68-69].

$$2jkn_0 \frac{\partial}{\partial z}\begin{bmatrix}\phi_x \\ \phi_y\end{bmatrix} = \begin{bmatrix}P_{xx} & P_{xy} \\ P_{yx} & P_{yy}\end{bmatrix}\begin{bmatrix}\phi_x \\ \phi_y\end{bmatrix} \tag{2-40}$$

where P_{xx} and P_{xy} are complex differential operators for ϕ_x and P_{yx} and P_{yy} for ϕ_y, the components of the operator P are

$$\begin{aligned}
P_{xx} &= \frac{\partial}{\partial x}\left[\frac{1}{n^2}\frac{\partial}{\partial x}n^2\right] + \frac{\partial^2}{\partial y^2} + k^2\left(n^2 - n_0^2\right) \\
P_{yy} &= \frac{\partial}{\partial y}\left[\frac{1}{n^2}\frac{\partial}{\partial y}n^2\right] + \frac{\partial^2}{\partial x^2} + k^2\left(n^2 - n_0^2\right) \\
P_{xy} &= \frac{\partial}{\partial x}\left[\frac{1}{n^2}\frac{\partial}{\partial y}n^2\right] - \frac{\partial^2}{\partial x \partial y} \\
P_{yx} &= \frac{\partial}{\partial x}\left[\frac{1}{n^2}\frac{\partial}{\partial x}n^2\right] - \frac{\partial^2}{\partial x \partial y}
\end{aligned} \tag{2-41}$$

The simplification $P_{xy} = P_{yx} = 0$ gives the important semi-vectroial approximation. Ignoring account P_{xy} and P_{yx} for polarization coupling. In this condition the transverse components are decoupled, simplifying the problem considerable while retaining what are usually the most significant polarization effects. The adjacent waveguide coupling for arrayed waveguide grating device is weak hence simulation by the semi-vectorial approximation is a great choice.

2-4-2 Typical Arrayed Waveguide Grating

We study 64 × 64 AWG with considering TE and TM modes. The fundamental mode is used as our initial mode to simulate the propagation condition for 64 Ｘ 64 arrayed waveguide grating based on the simulator WDM_PHASER [70]. From the Fig. 2-4, we find all outputs have uniform power distribution. Fig. 2-5 shows TM mode simulation result of transmission spectra of a 64 channel AWG. The insertion loss and crosstalk for TE and TM modes versus the wavelength are shown in Fig. 2-6. We simulate the power loss and scan the wavelength from 1535nm to 1565nm as shown in Fig. 2-6. According to the preliminary simulation results, we can get average insertion loss for TE and TM modes are 5.5dB and 5.3dB, respectively. The crosstalk to the neighbouring channels for TE and TM modes are –19.5dB and –19.9dB, respectively. The insertion loss of our prototype 64 × 64 channel AWG is 5.4dB in average. Assuming launching the fundamental mode as our initial mode propagating along these waveguides, the bandwidth level is –30dB, the uniformity of these devices is 1.64dB, and the maximum bending loss in 266 channel waveguides of the PAW of the AWG is 0.093dB in accordance of the simulation regulations.

According to the simulation results, the maximum transmission loss of the array waveguide grating is –0.2dB. The theoretical 3dB bandwidth and insertion losses are 21.3GHz and 3dB, respectively.

The theoretical insertion loss is due to the diffraction loss in the first slab region and imperfect focusing loss in the second slab region. Both of them are caused by two factors: the finite number of arrayed waveguides, and the waveguide gap between PAWs at the slab- array interface which can be made by the lithography process.

2-4-3 Study and Analysis the Waveguide Separation of Phased Array Waveguides

AWG technologies have attracted lots of attentions recently [71]. The AWG with low insertion loss, high stability, and good mass producible are the most promising devices for multi/demultiplexers or filter in wavelength division multiplexing (WDM) systems [72]. AWG devices are already become the necessary elements in WDM optical communication systems. The insertion loss of our prototype 64╳64 channel AWG, is the average value around 5.5 dB, and has two primary causes. One is the insertion loss is from fiber-to-waveguide coupling loss, caused by the field mismatch between a fiber and a waveguide. The other is the transition loss that occurs at the junction between FPR and arrayed waveguides. This is because there are gaps between PAW at the junction; this leads to a field mismatch between the FPR and PAW. The gap size is limited by the finite resolution of the fabrication process. We define the gap size of the PAW at the junction of FPR is d_{PA} as shown in Fig. 2-7. The variation range of the PAW separation d_{PA} is from 6.6μm to 7.8μm, limited by the width of FPR and the bending radius of PAWs. [The geometric value of the FPR is based on the specifications in optical network that we defined such as: I/O channel number、channel spacing、uniformity.] Fig. 2-8 (a)-(m) represents the relation between transmittance and crosstalk for 64 output channel with different d_{PA} from 6.6 μm to 7.8 μm. For different values of d_{PA}, the transmittance and crosstalk at 64 output channels are different, the crosstalk value is increasing when the waveguide separation at PAW d_{PA} arising from 7.3 to 7.8μm, and the transmittance variation is minor before d_{PA} = 7.2μm, and from d_{PA} = 7.3 to 7.8μm, the transmittance variation increases. We try to find the optimum value d_{PA} for all output channels. Fig. 2-9 shows the relation of transmission, crosstalk and uniformity with d_{PA}, the deviation of the relative crosstalk is small at d_{PA} = 7.2μm, but the relative insertion loss is higher than the value for d_{PA} = 7.3μm. At d_{PA} = 7.3μm, the deviation of relative insertion loss is small, although the crosstalk is a little higher than the value for d_{PA} = 7.2μm, the uniformity is good, thus we find the d_{PA} = 7.3μm is an optimum value. At d_{PA} = 7.3μm, the average transmittance and crosstalk of 64 channel is －4dB and －23dB, respectively, and the uniformity is 0.6. Hence, we chose d_{PA} = 7.3μm as the separation of the waveguide at the junction of FPR and PAW. Fig. 2-10 is one of our simulation results showing transmittance spectrum of the 64×64 arrayed waveguide grating based on SOI with waveguide separation d_{PA} = 7.3μm. This result demonstrates the channel spacing 50GHz centered at 1550nm wavelength. The insertion loss is in the range of 3.7dB~5.5dB. The crosstalk is controlled between －21dB and －25dB, and the back ground noise is controlled under －30dB.

2-4-4 Design and Analysis of Tapered Waveguide at the Junction of Input/Output Port and Free Propagation Region

After we have find out a compromise value d_{PA} (=7.3μm) of the separation at the junction between PAWs and FPR, the crosstalk value is not good enough for DWDM system applications. Hence, we improve the crosstalk value by adding tapered waveguide at the junction of the input/output waveguide and the FPR. Tapered structure at waveguide let the optical field propagation at the transition region smoothly. The light output from a FPR can make matching propagation into the waveguide array and then passing through the tapered waveguides, and vice versa. Fig. 2-11 shows the structure of our designed tapered waveguide, with the start width W_{taper} and fixed end width 5.3μm, the taper region is linearly increasing with tapered length =100μm. For tapered length L_{taper} = 100 μm to scrutinize W_{taper} from 5.4 μm to 7.3 μm are shown in Fig. 2-12 (a)~(t), when the W_{taper} arise from 5.3 μm to 7.3 μm the average variation of transmission is less than 1 dB, but the average crosstalk value for 64 output port has violent change from –23 dB to –33 dB with different W_{taper} value, we find at the L_{taper}= 100 μm and W_{taper} = 7.2 μm shown in Fig. 2-13, the average crosstalk value for 64 output channel of arrayed waveguide grating is reducing to –33 dB and insertion loss in decrease from 3.9 dB to 2.93 dB by adding the tapered structure at the junction of the input/output waveguide and free propagation region. Fig. 2-14 shows the transmittance spectra of regular AWG and tapered AWG. For applying tapered AWG, the transmittance is improved 1dB averagely compared with the regular AWG. The inter-channel crosstalk of tapered AWG is averagely improved 10dB. As shown in Fig. 2-15, maximum 20dB crosstalk reduction can be achieved at wavelength 1547nm. The final transmittance spectrum of the improved 64×64 channel AWG with tapered waveguide is shown in Fig. 2-16. The lowest transmittance spectrum is improved below 2.2dB. The crosstalk is controlled in the region of －40dB to －30dB and the background noise is designed below －35dB. These results show the successful design of improving the characteristics of 64×64 AWG.

2-5 Summary

The AWG plays a crucial role in the realization of modern optical networks. In this chapter, we described the basic operation of the AWG and summarized the methods used for AWG design. However it is highlighted that current methods of analysis do not accurately predict effects observed in fabricated structures, such as increased channel crosstalk.

Furthermore, we have found a tradeoff value of waveguide separation (d_{PA} = 7.3μm) at junction between arrayed waveguide and free propagation region. With this searched parameter, we can get a better uniformity for 64×64 AWG channel output spectrum transmittance with considering of compromising value for insertion loss and crosstalk. Then, we apply tapered waveguide structure design at the junction between input/output waveguide and the FPR. This work successfully improved the transmittance spectrum and crosstalk reduction from 5dB and –20dB to 2.93dB and –33dB, respectively, for a 64×64 AWG based on SOI substrate with 50GHz channel spacing centered at wavelength 1550nm. It is believed that such a device can be applied in DWDM optical interconnection and communication systems. These results are quite useful for the experimental works in the future. In the advance research, we expect to realize the 64×64 WDM MUX AWG for applying in a DWDM high capacity metropolitan area optical communication networks.

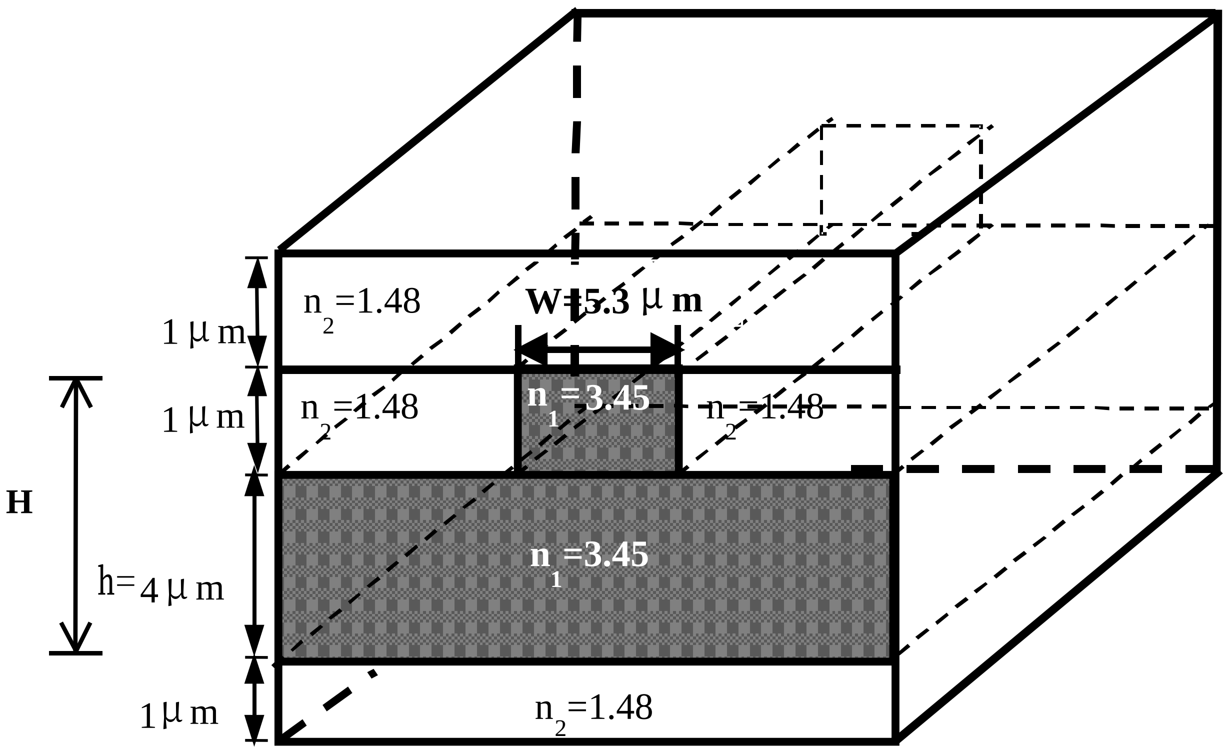

Fig. 2-1 Schematic diagram of a embedded channel SOI waveguide AWG

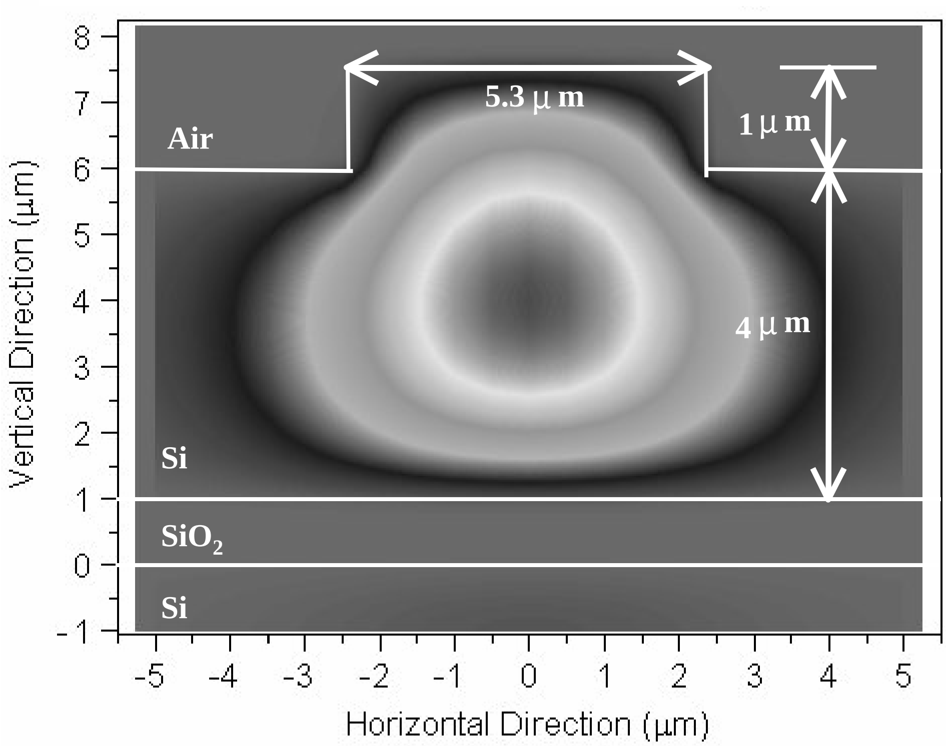

Fig. 2-2 The mode pattern of the single mode waveguide

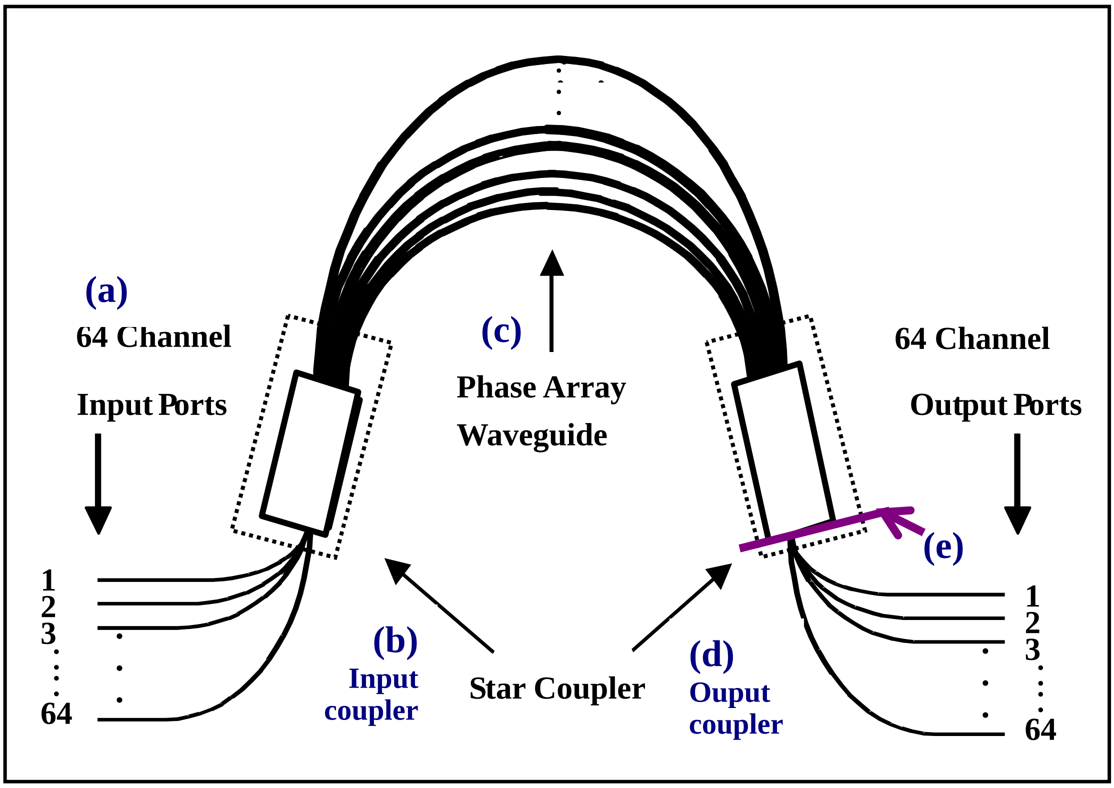

Fig. 2-3 Top view of the multichannel AWG

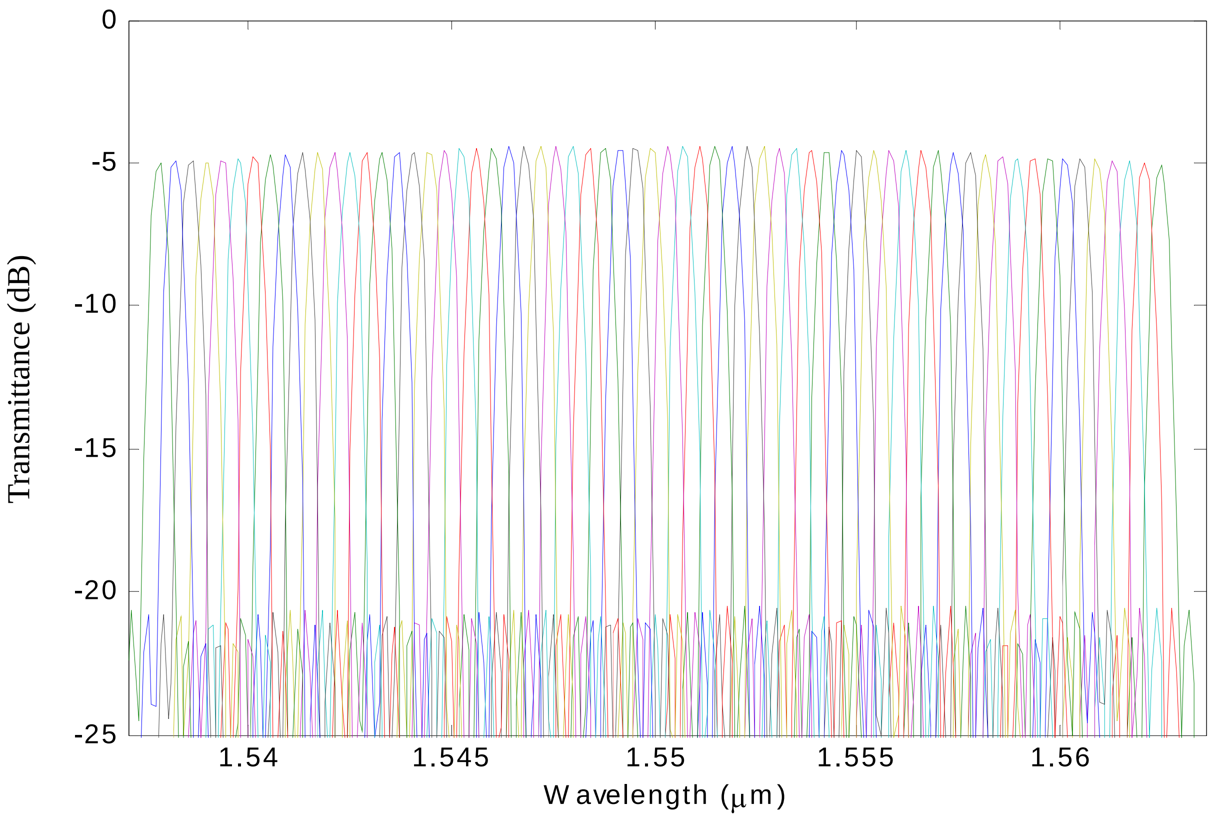

Fig. 2-4 TE mode simulation result of transmission spectra of a 64 channel AWG

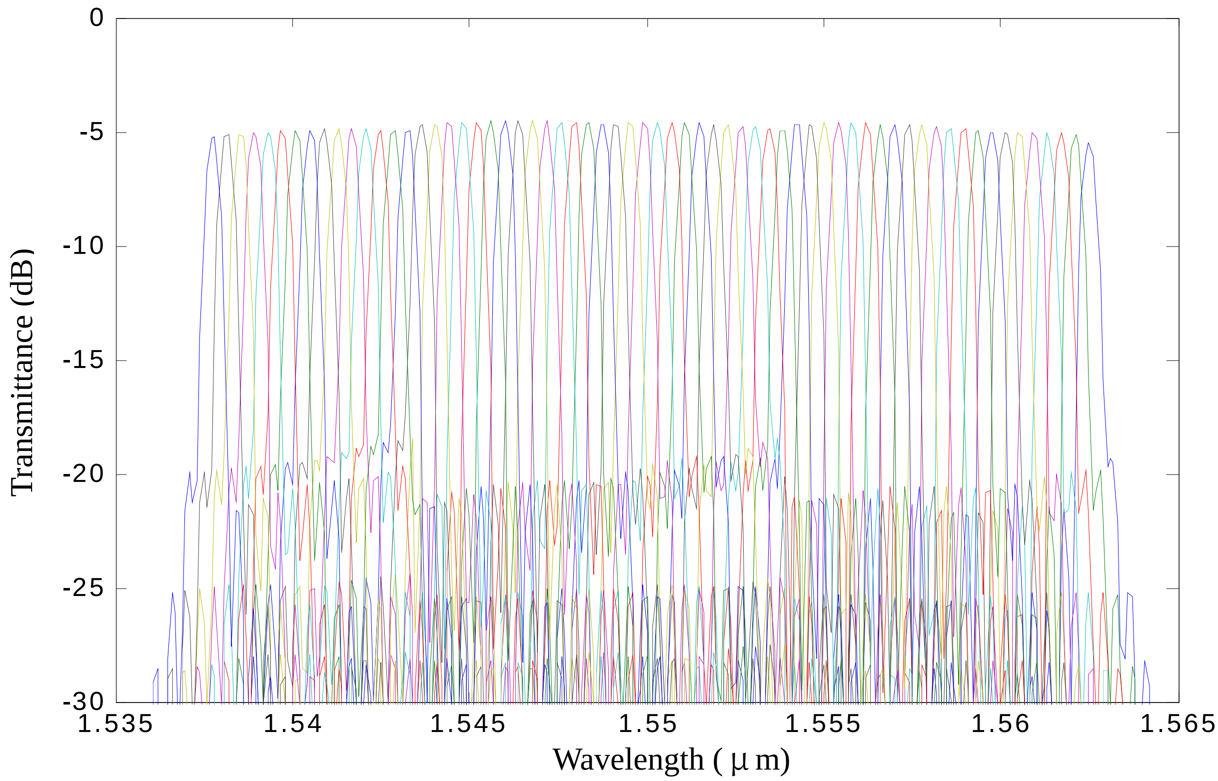

Fig. 2-5 TM mode simulation result of transmission spectra of a 64 channel AWG

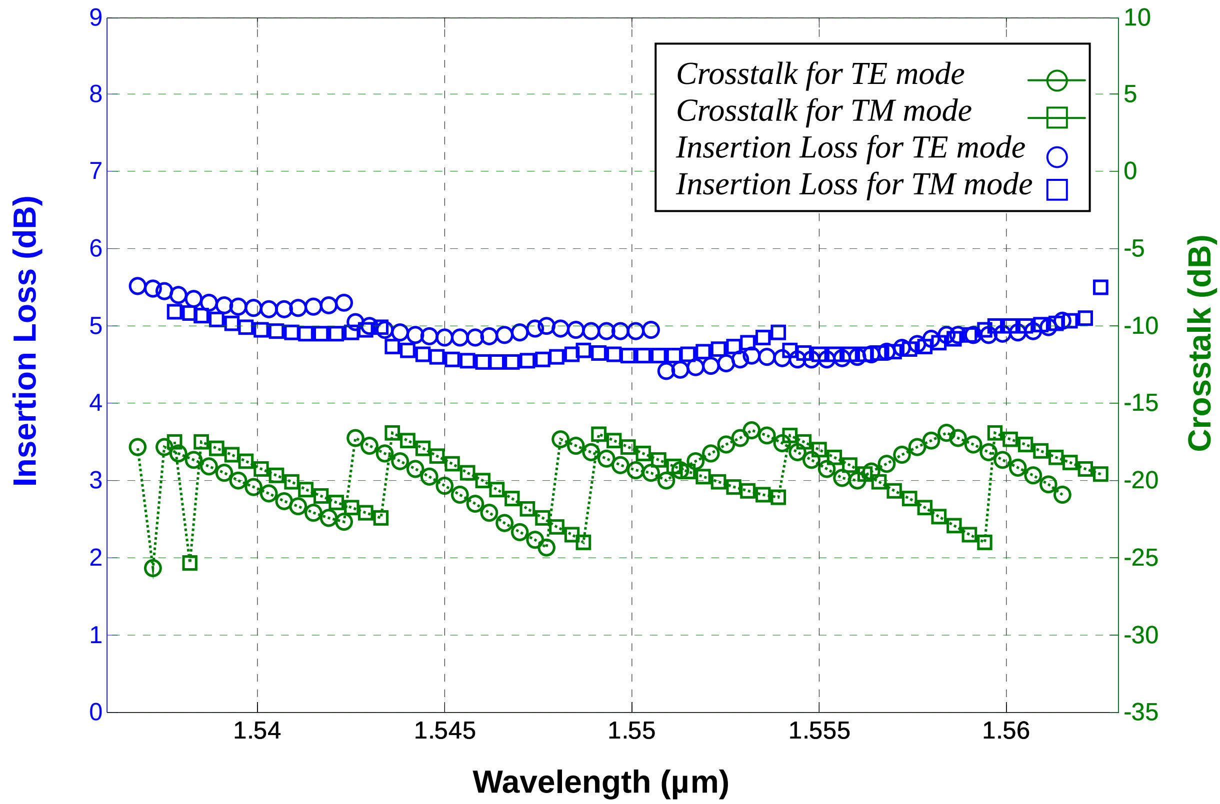

Fig. 2-6 The insertion loss and the crosstalk for TE mode and TM mode versus wavelength

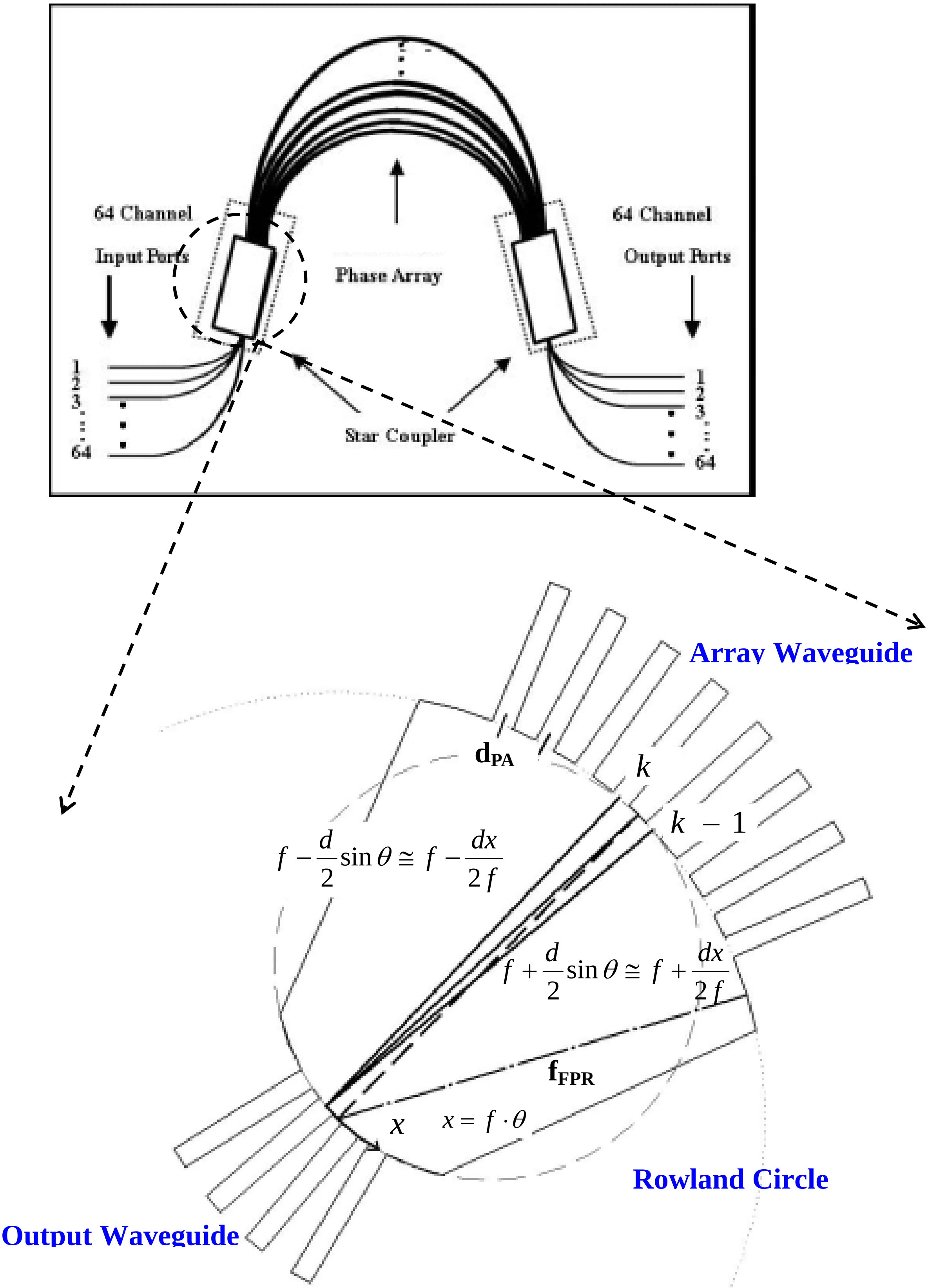

Fig. 2-7 Enlarge view of Free Propagation Region of Arrayed Waveguide Grating

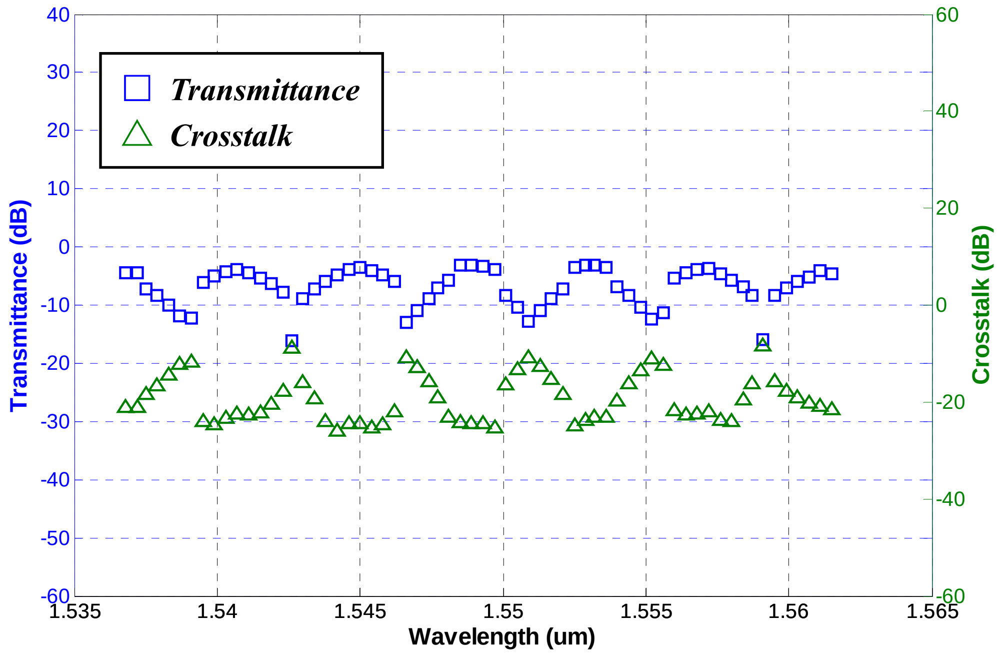

(a) Transmission and crosstalk value at d_{PA}=6.6μm

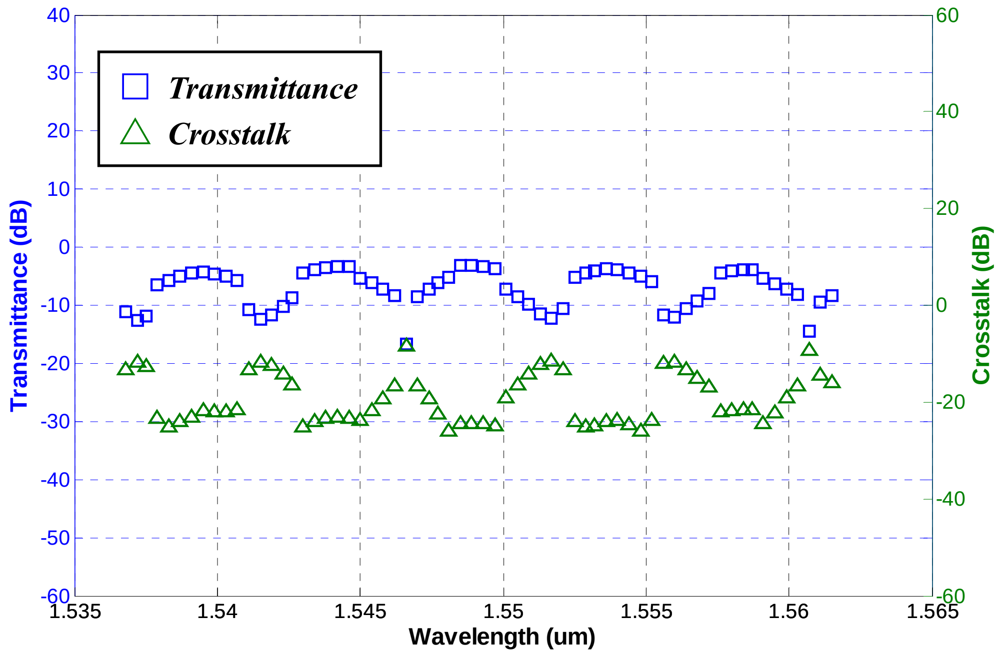

(b) Transmission and crosstalk value at d_{PA}=6.7μm

Fig. 2-8 The transmission and crosstalk value of the Arrayed Waveguide Grating with different waveguide separation (d_{PA}) at phased array waveguide (a) d_{PA} =6.6 μ m (b) d_{PA} =6.7 μ m

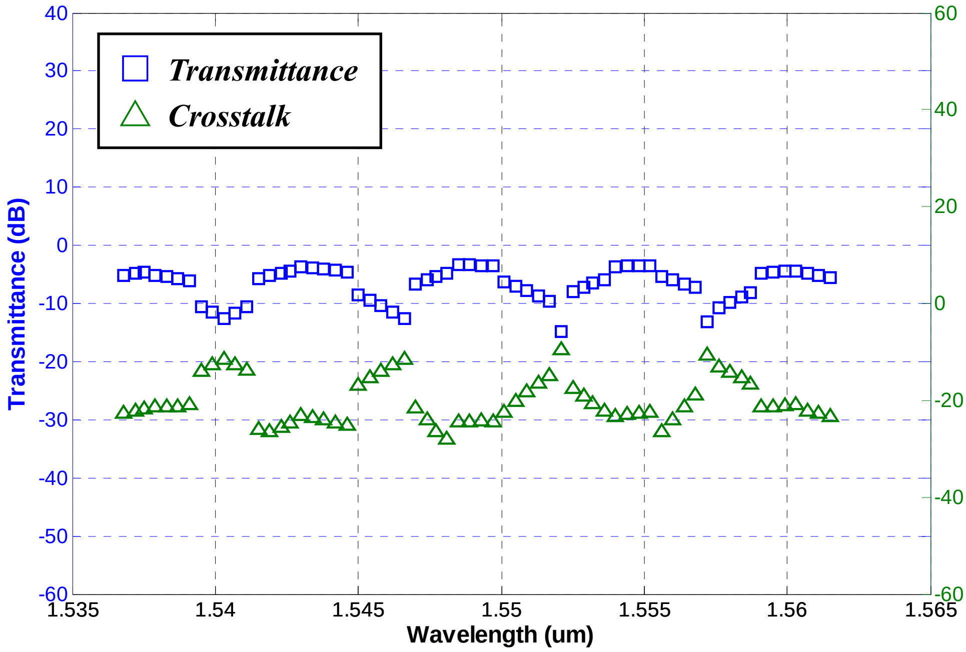

(c) Transmission and crosstalk value at $\boldsymbol{d_{PA}}$=6.8μm

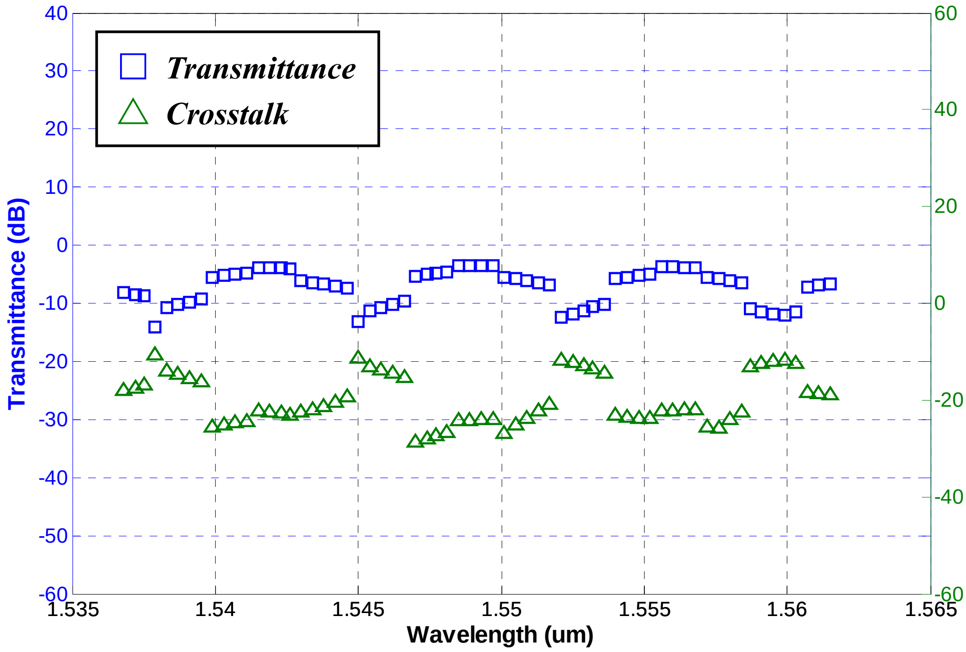

(d) Transmission and crosstalk value at $\boldsymbol{d_{PA}}$=6.9μm

Fig. 2-8 The transmission and crosstalk value of the Arrayed Waveguide Grating with different waveguide separation (d_{PA}) at phased array waveguide (c) $\boldsymbol{d_{PA}}$ =6.8μm (d) $\boldsymbol{d_{PA}}$ =6.9μm

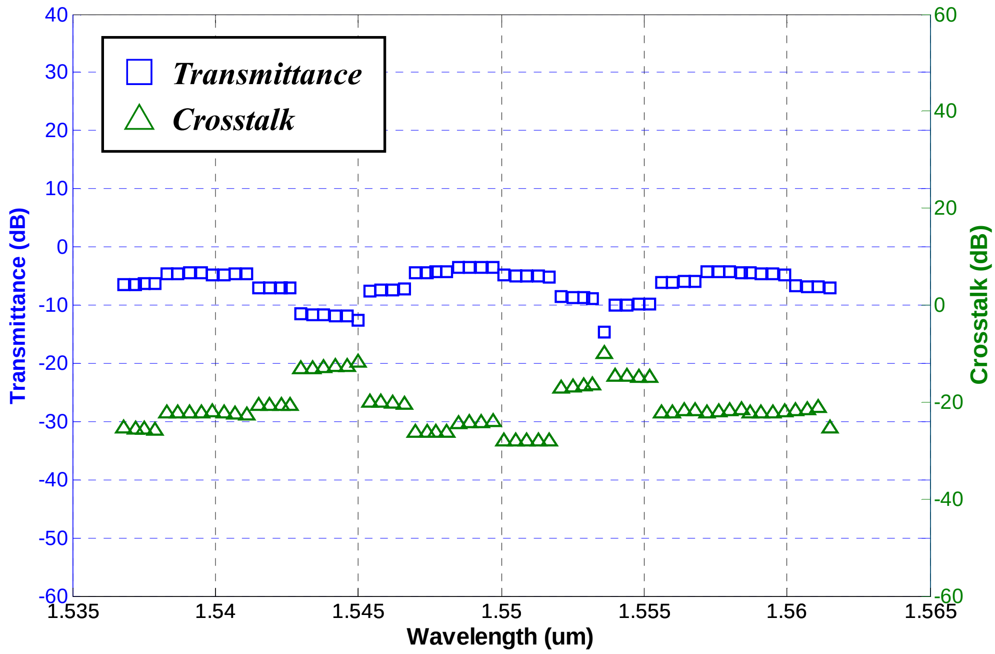

(e) Transmission and crosstalk value at d_{PA}=7μm

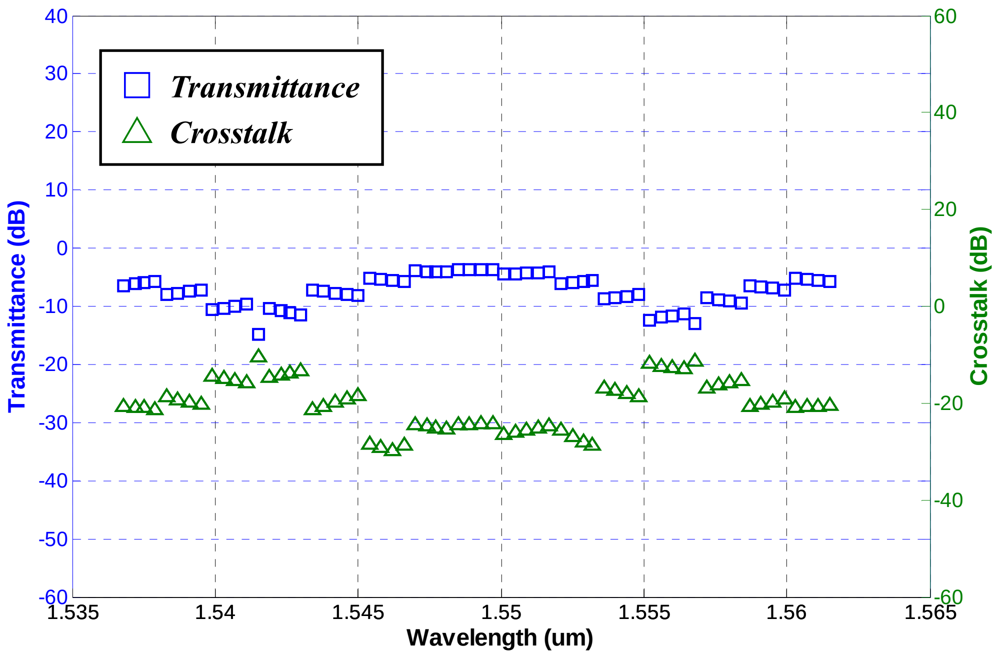

(f) Transmission and crosstalk value at d_{PA}=7.1μm

Fig. 2-8 The transmission and crosstalk value of the Arrayed Waveguide Grating with different waveguide separation (d_{PA}) at phased array waveguide (e) d_{PA} =7μm (f) d_{PA} =7.1μm

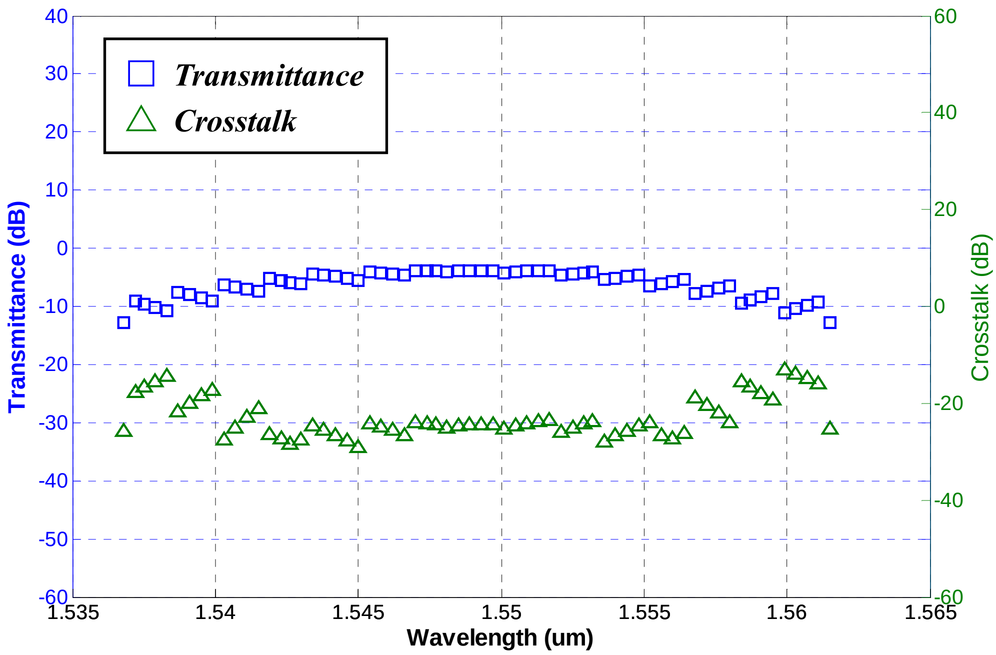

(g) Transmission and crosstalk value at d_{PA}=7.2μm

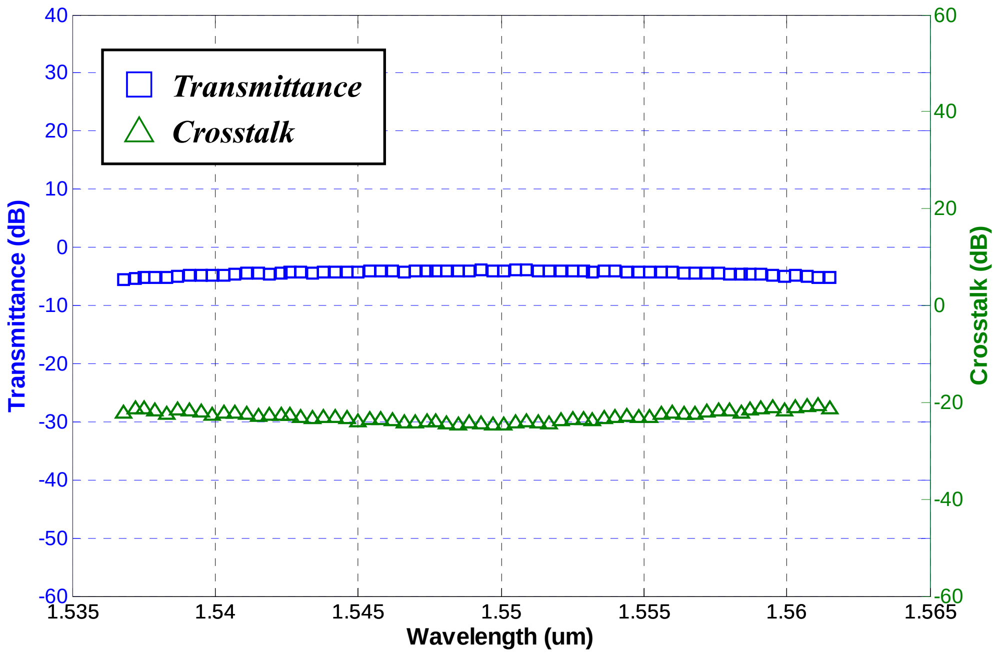

(h) Transmission and crosstalk value at d_{PA}=7.3μm

Fig. 2-8 The transmission and crosstalk value of the Arrayed Waveguide Grating with different waveguide separation (d_{PA}) at phased array waveguide (g) d_{PA} =7.2 μm (h) d_{PA} =7.3 μm

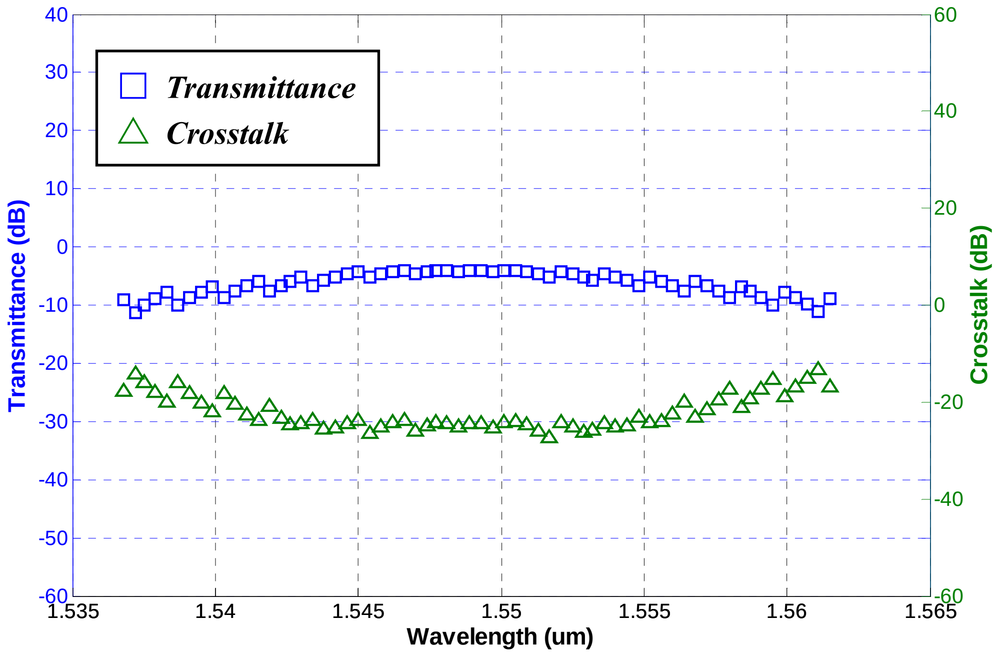

(i) Transmission and crosstalk value at $\boldsymbol{d_{PA}}$=7.4μm

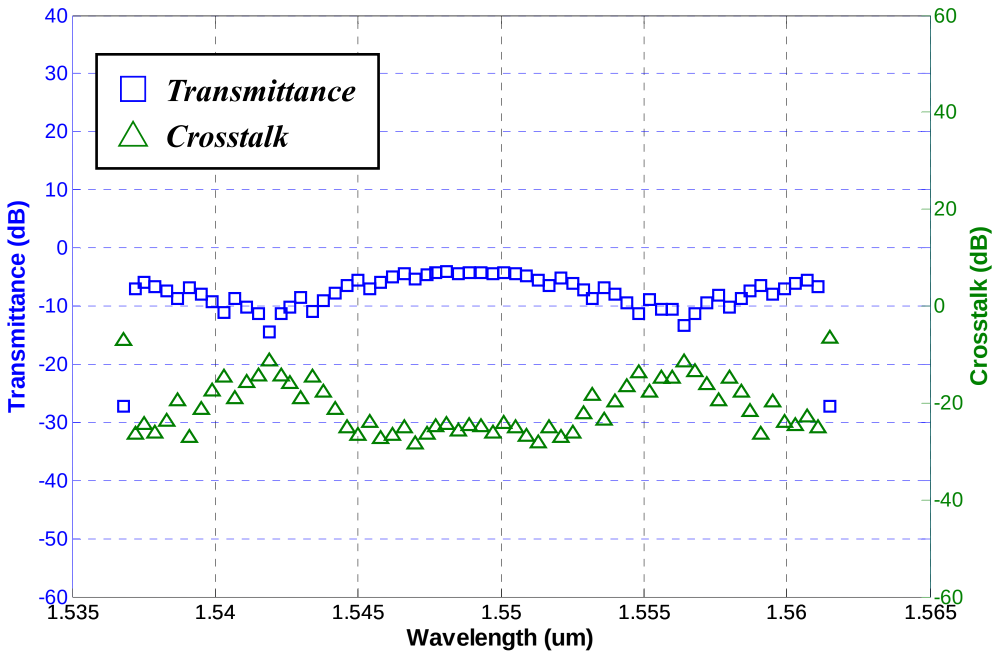

(j) Transmission and crosstalk value at $\boldsymbol{d_{PA}}$=7.5μm

Fig. 2-8 The transmission and crosstalk value of the Arrayed Waveguide Grating with different waveguide separation (d_{PA}) at phased array waveguide (i) $\boldsymbol{d_{PA}}$ =7.4 μm (j) $\boldsymbol{d_{PA}}$ =7.5 μm

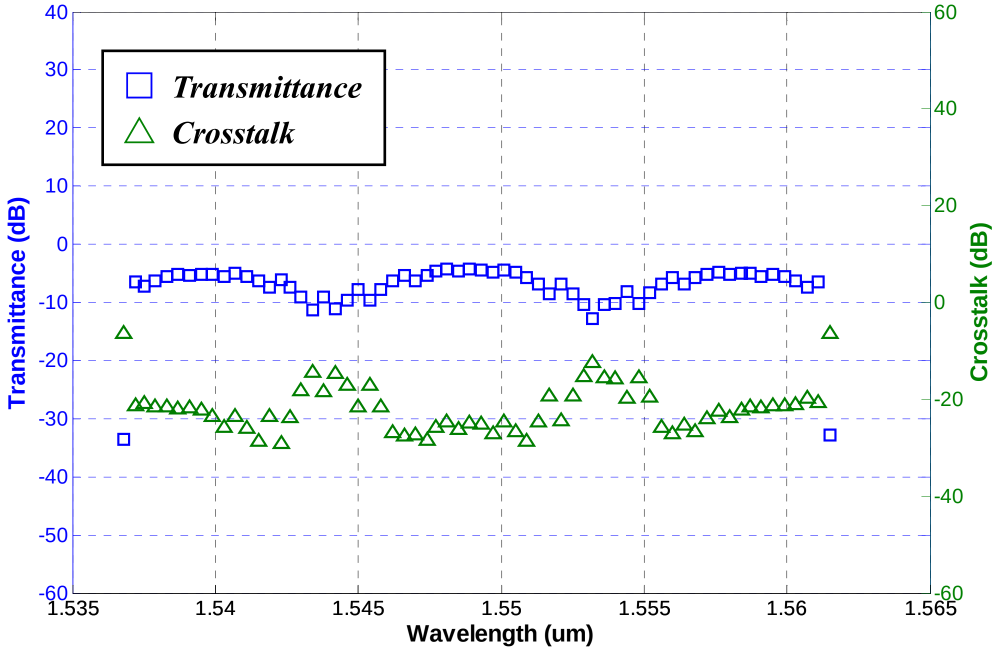

(k) Transmission and crosstalk value at d_{PA}=7.6μm

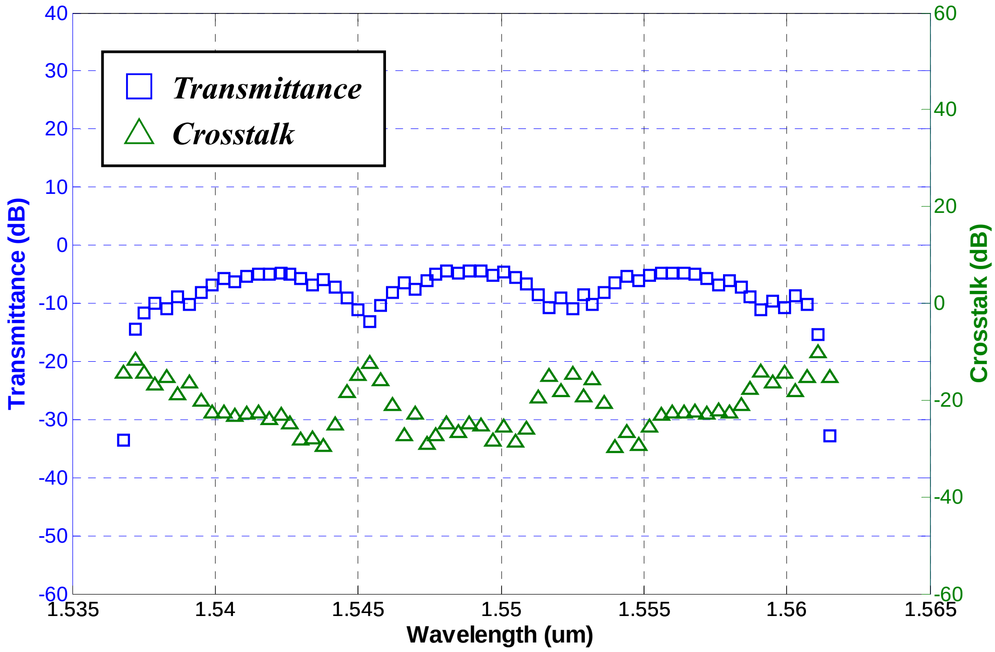

(l) Transmission and crosstalk value at d_{PA}=7.7μm

Fig. 2-8 The transmission and crosstalk value of the Arrayed Waveguide Grating with different waveguide separation (d_{PA}) at phased array waveguide (k) d_{PA} =7.6 μm (l) d_{PA} =7.7 μm

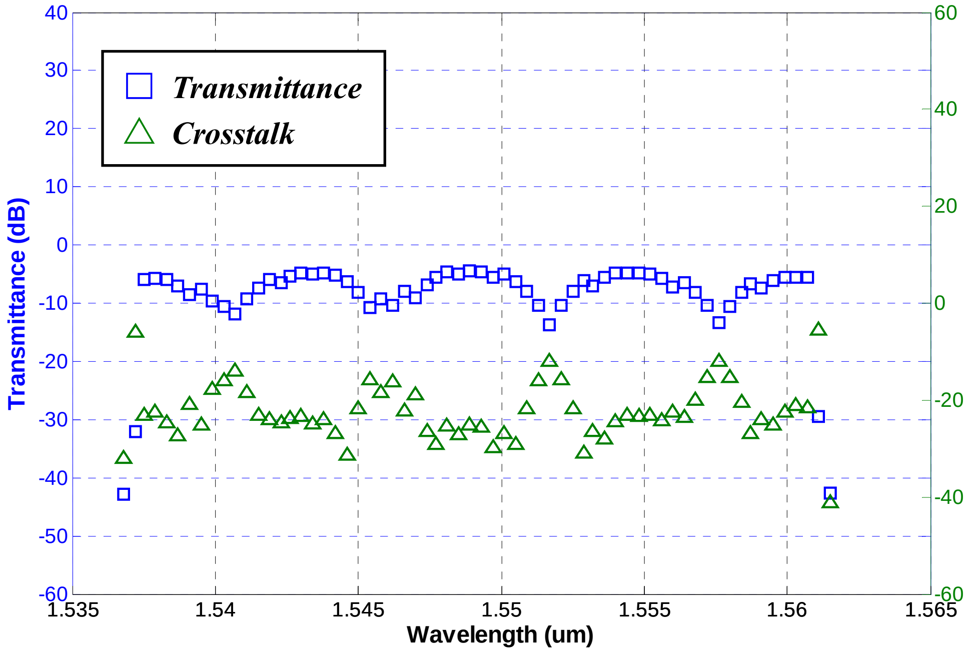

(m) Transmission and crosstalk value at $\boldsymbol{d_{PA}}$=7.8μm

Fig. 2-8 The transmission and crosstalk value of the Arrayed Waveguide Grating with different waveguide separation (d_{PA}) at phased array waveguide (m) $\boldsymbol{d_{PA}}$ =7.8 μ m

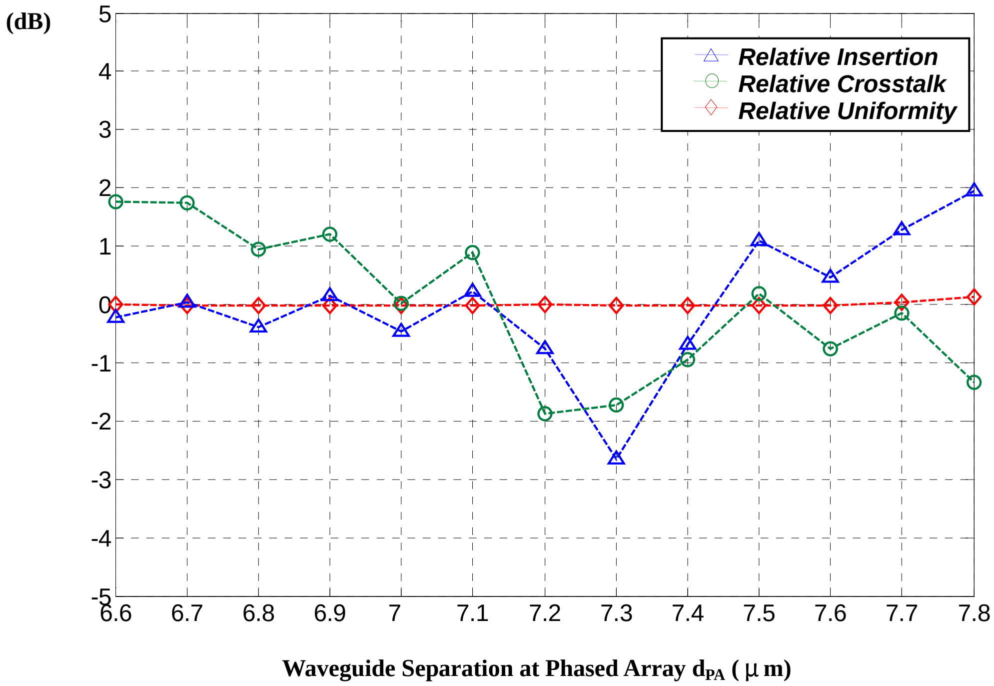

Fig. 2-9 Relation of transmission, crosstalk and uniformity with d_{PA}

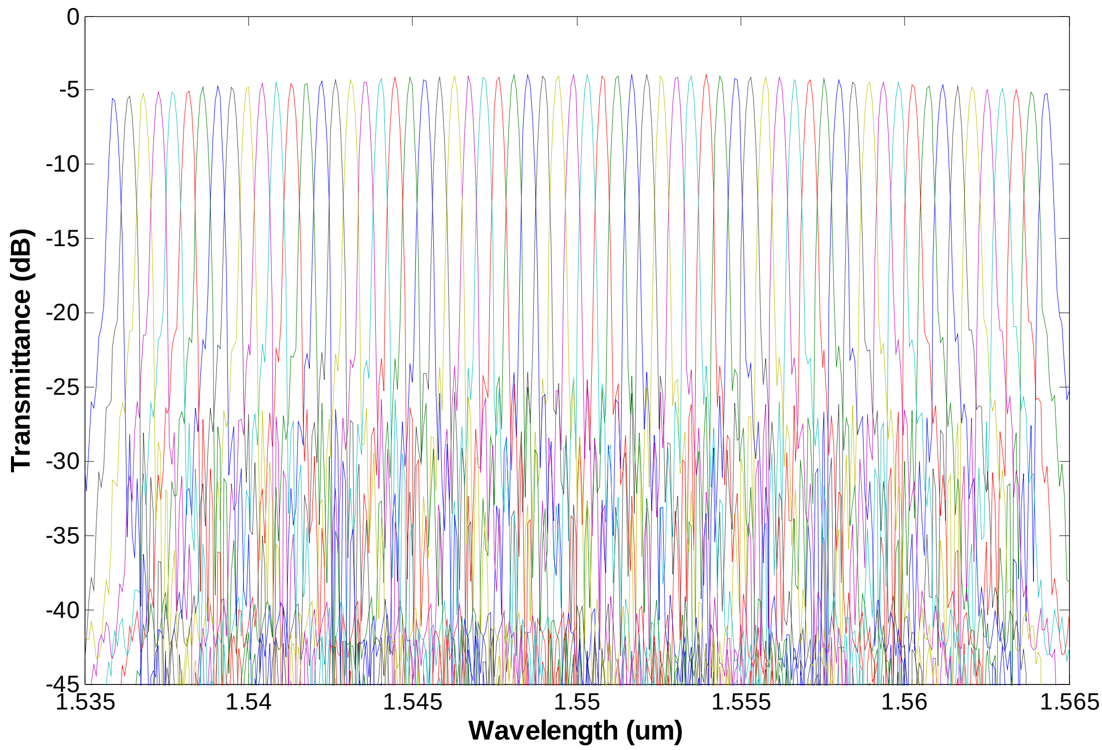

Fig. 2-10 Transmittance spectrum with d_{PA}=7.3 μ m

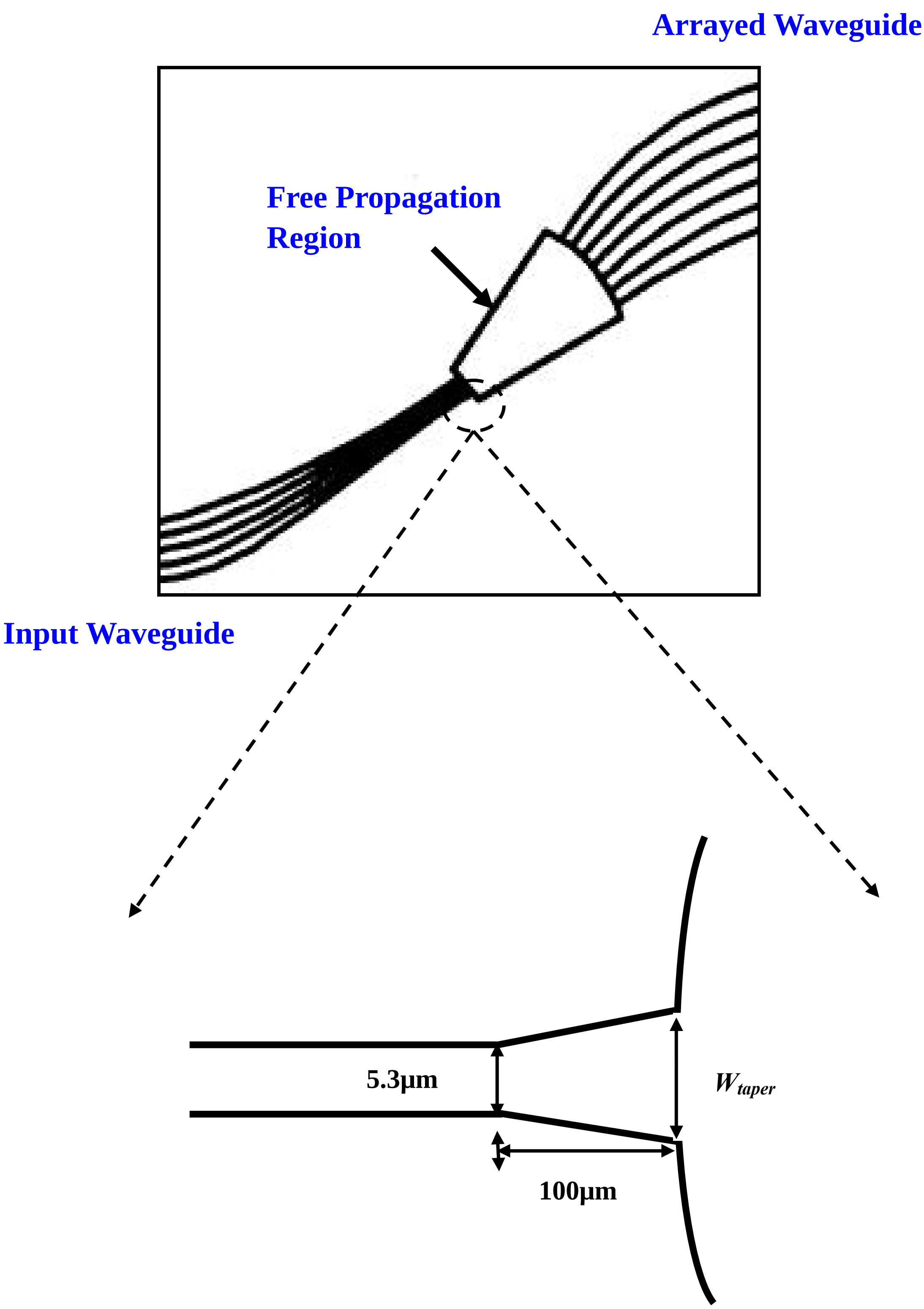

Fig. 2-11 Structure of the tapered waveguide at input/output waveguide of AWG

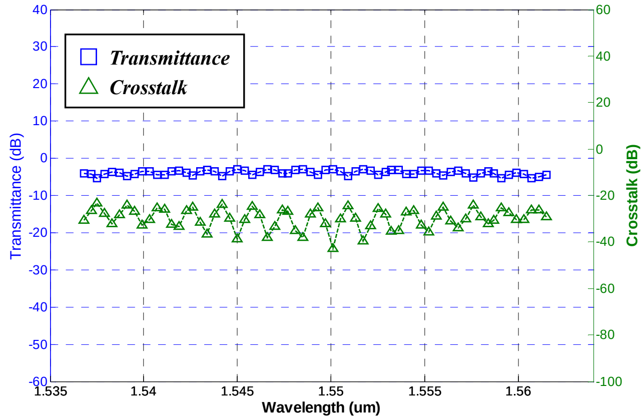

(a) $\boldsymbol{W_{taper}}$ = 5.4μm

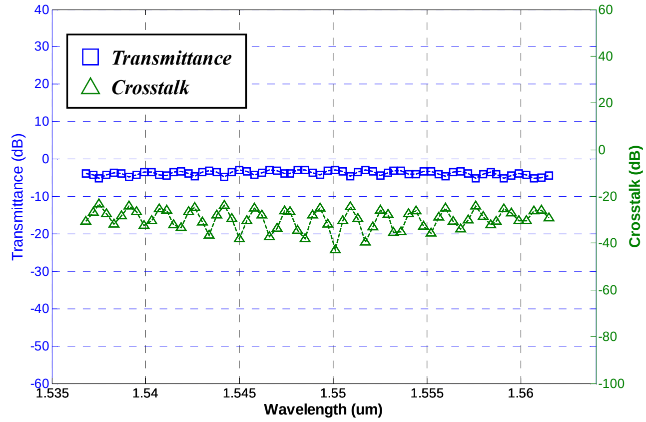

(b) $\boldsymbol{W_{taper}}$ = 5.5μm

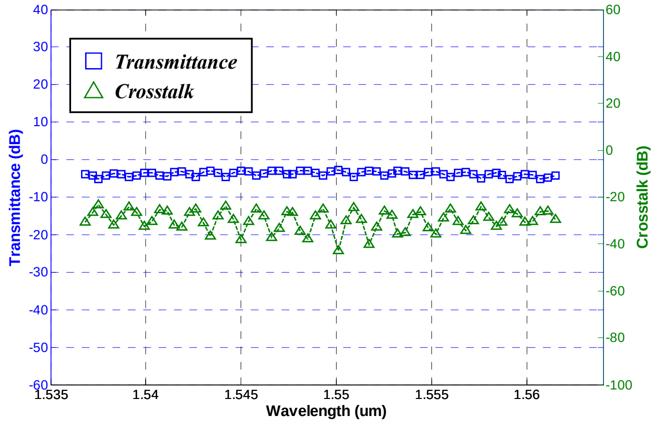

(c) $\boldsymbol{W_{taper}}$ = 5.6μm

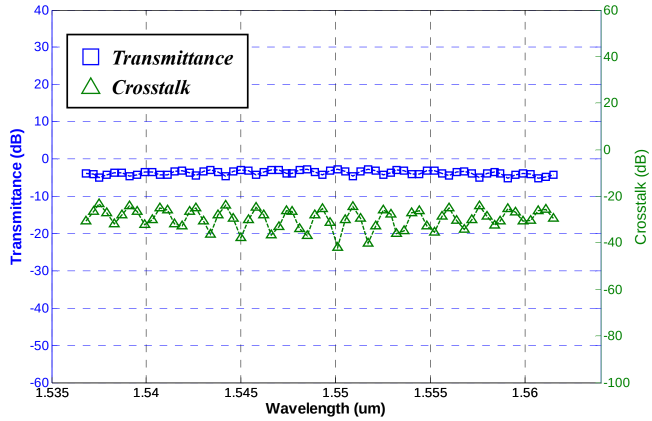

(d) $\boldsymbol{W_{taper}}$ = 5.7μm

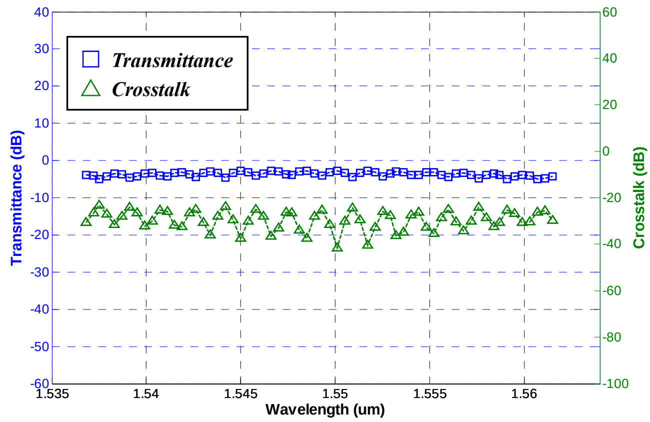

(e) $\boldsymbol{W_{taper}}$ = 5.8μm

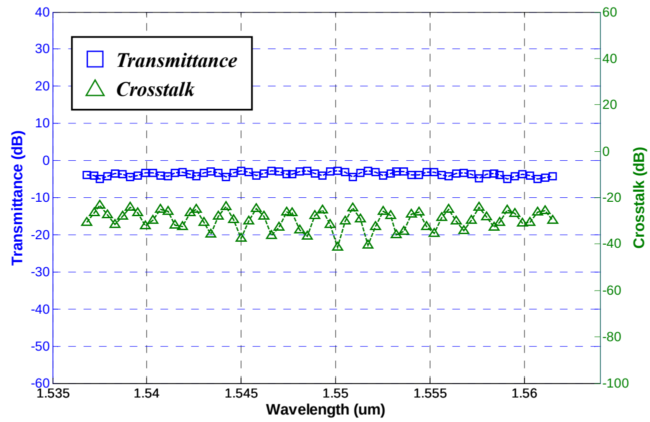

(f) $\boldsymbol{W_{taper}}$ = 5.9μm

Fig. 2-12 The transmittance and crosstalk value of the arrayed waveguide grating with different tapered width (W_{taper}) at input/output port (a) W_{taper} =5.4 μ m (b) W_{taper} =5.5 μ m (c) W_{taper} =5.6 μ m (d) W_{taper} =5.7 μ m (e) W_{taper} =5.8 μ m (f) W_{taper} =5.9 μ m

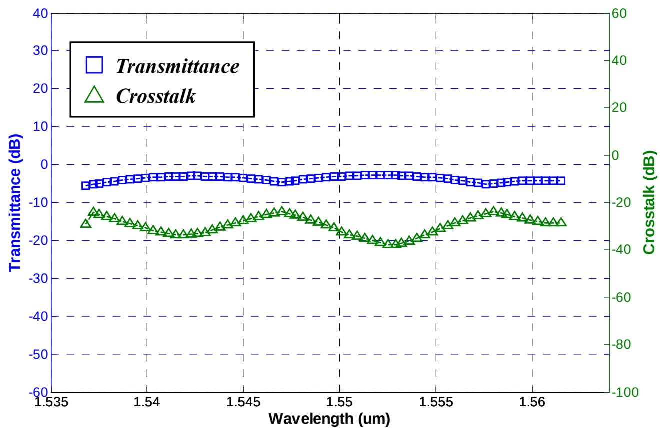

(g) $\boldsymbol{W_{taper}}$ = 6μm

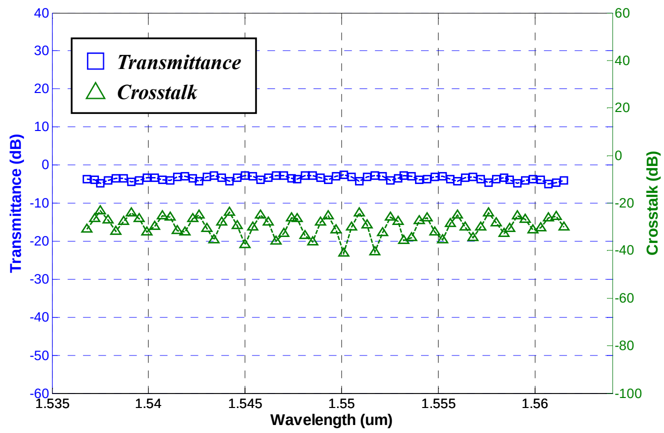

(h) $\boldsymbol{W_{taper}}$ = 6.1μm

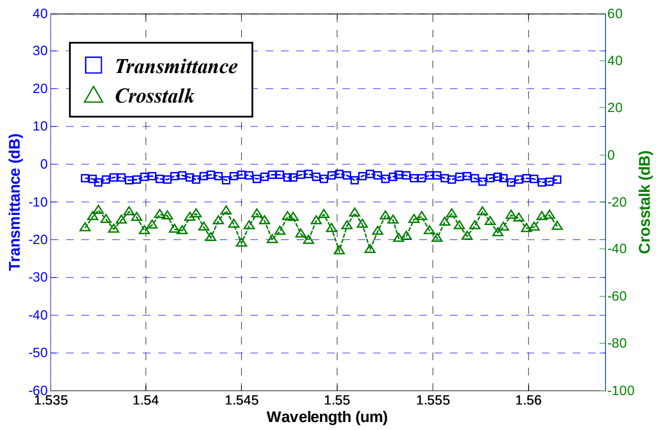

(i) $\boldsymbol{W_{taper}}$ = 6.2μm

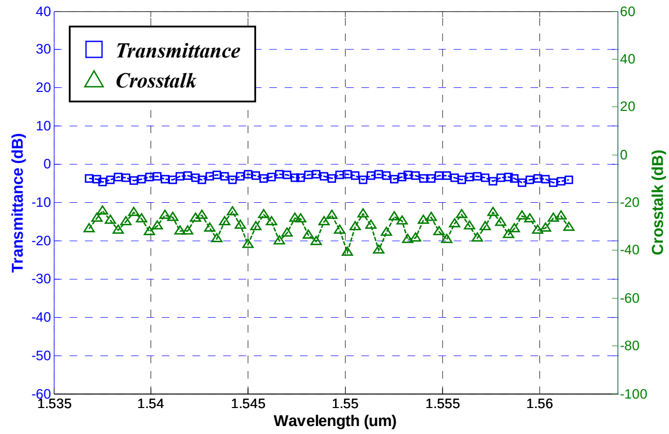

(j) $\boldsymbol{W_{taper}}$ = 6.3μm

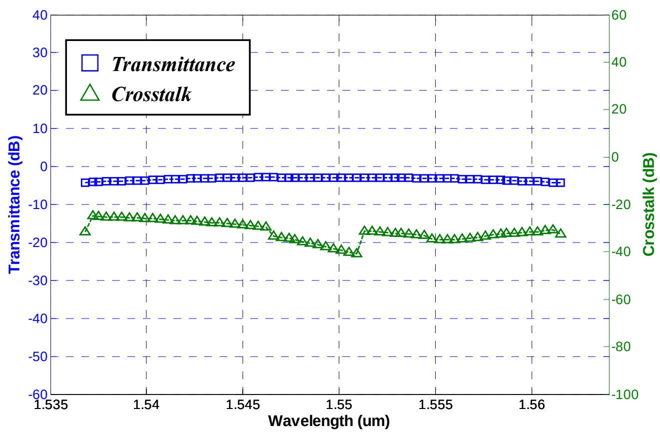

(k) $\boldsymbol{W_{taper}}$ = 6.4μm

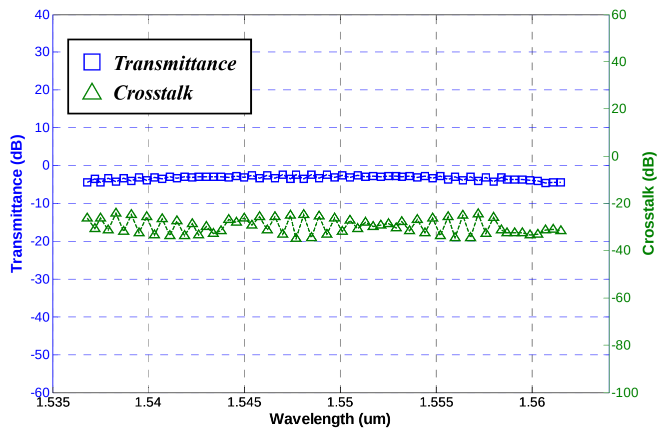

(l) $\boldsymbol{W_{taper}}$ = 6.5μm

Fig. 2-12 The transmittance and crosstalk value of the arrayed waveguide grating with different tapered width (W_{taper}) at input/output port (g) W_{taper} = 6 μm (h) W_{taper} = 6.1 μm (i) W_{taper} = 6.2 μm (j) W_{taper} = 6.3 μm (k) W_{taper} = 6.4 μm (l) W_{taper} = 6.5 μm

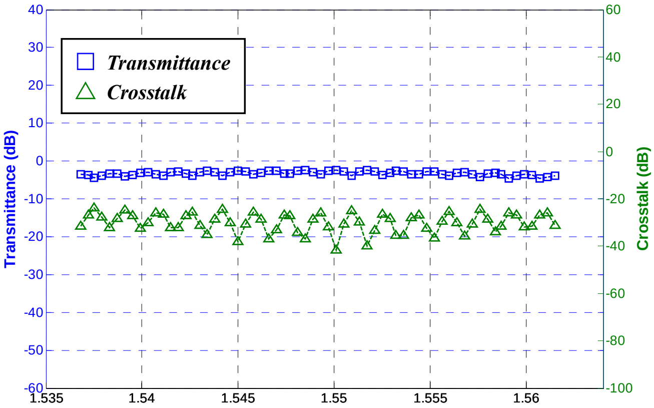

(m) W_{taper} = 6.6μm

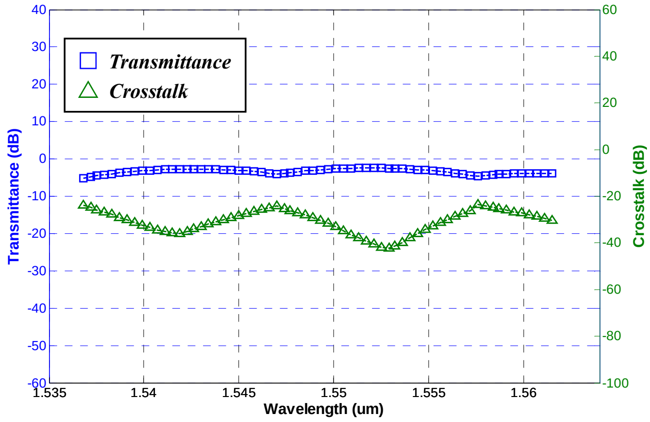

(n) W_{taper} = 6.7μm

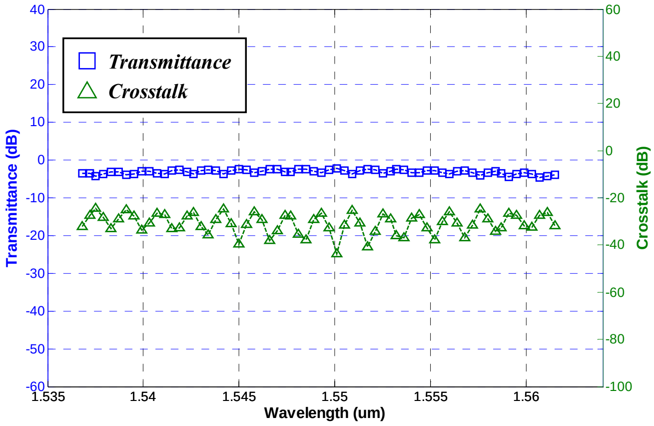

(o) W_{taper} = 6.8μm

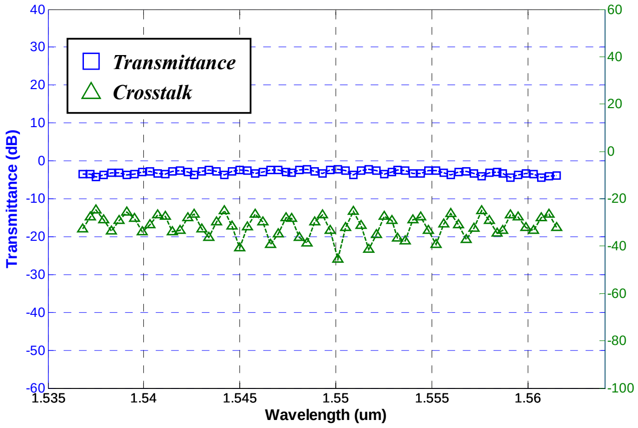

(p) W_{taper} = 6.9μm

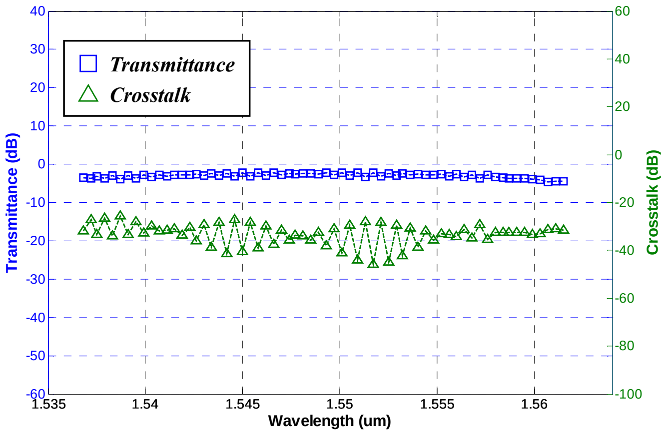

(q) W_{taper} = 7μm

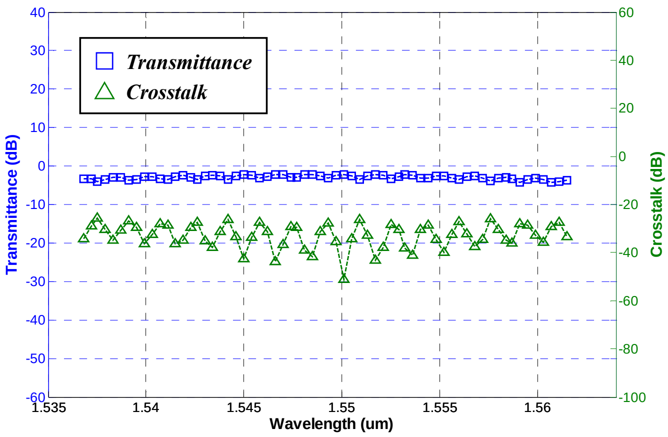

(r) W_{taper} = 7.1μm

Fig. 2-12 The transmittance and crosstalk value of the arrayed waveguide grating with different tapered width (W_{taper}) at input/output port (m) W_{taper} = 6.6 μm (n) W_{taper} = 6.7 μm (o) W_{taper} = 6.8 μm (p) W_{taper} = 6.9 μm (q) W_{taper} = 7 μm (r) W_{taper} = 7.1 μm

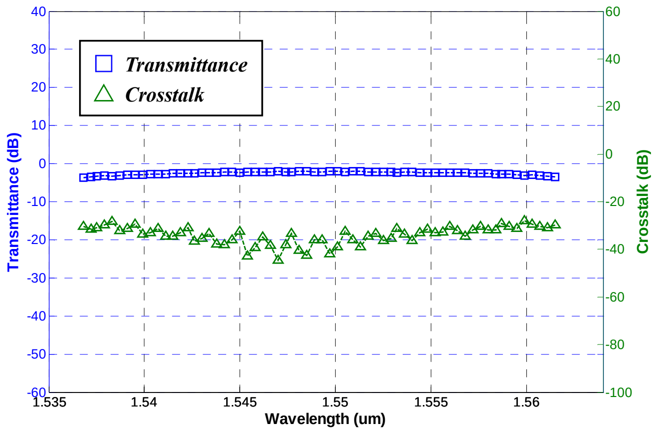

(s) W_{taper} = 7.2μm

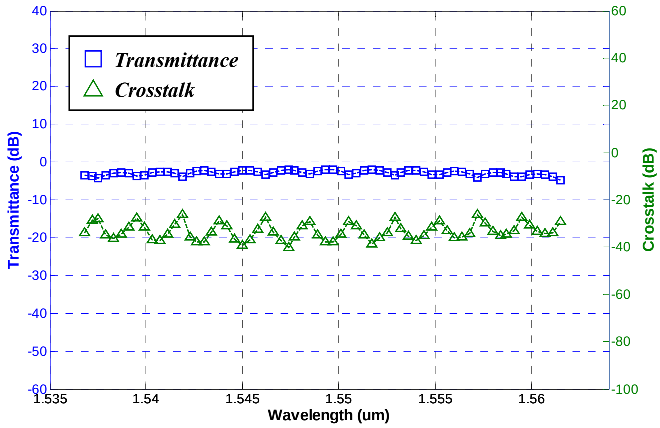

(t) W_{taper} = 7.3μm

Fig. 2-12 The transmittance and crosstalk value of the arrayed waveguide grating with different tapered width (W_{taper}) at input/output port (s) W_{taper} = 7.2 μ m (t) W_{taper} = 7.3 μ m

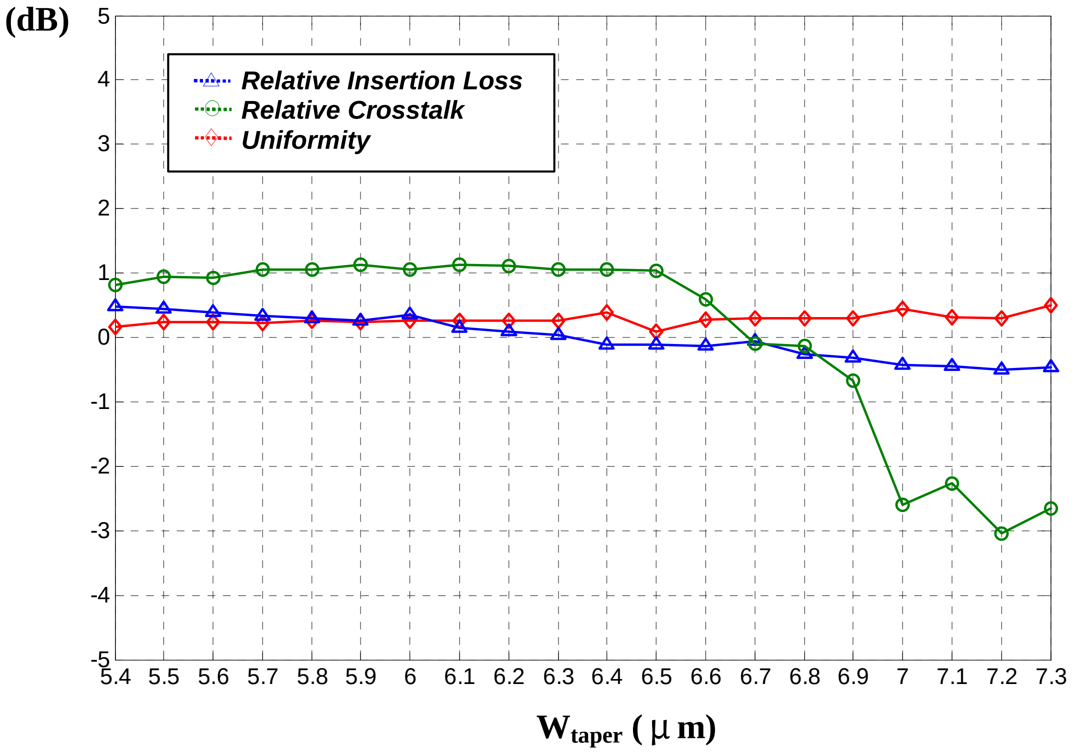

Fig. 2-13 Relation of transmission, crosstalk and uniformity of tapered AWG with different W_{taper} value

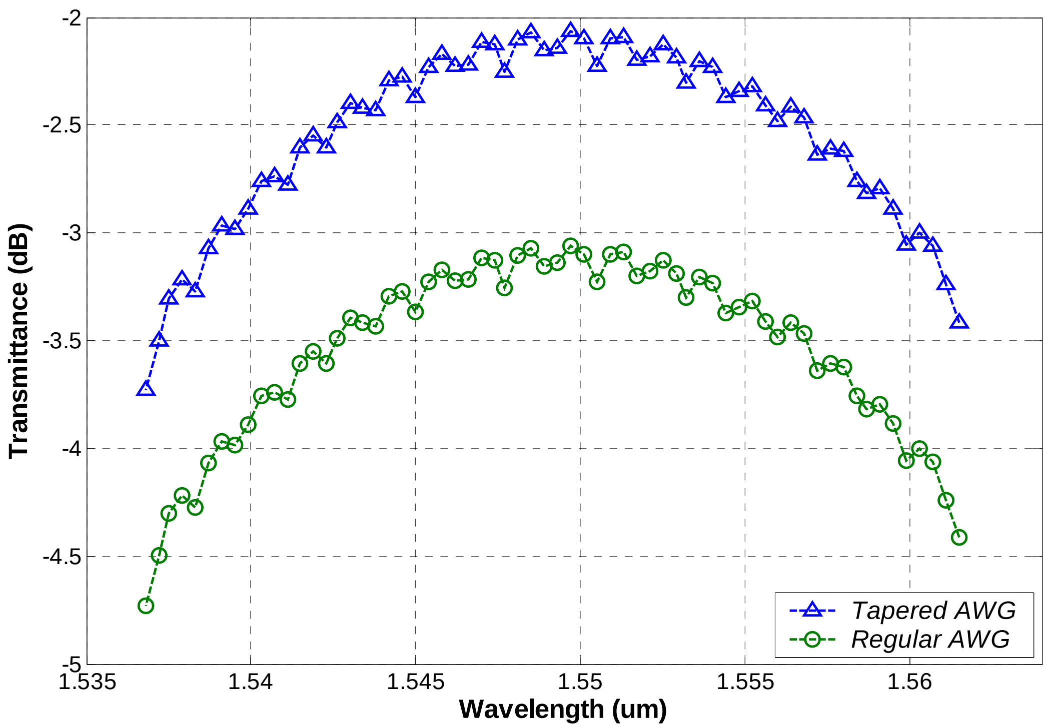

Fig. 2-14 Comparison of the transmittance for 64×64 regular AWG and 64×64 tapered-AWG

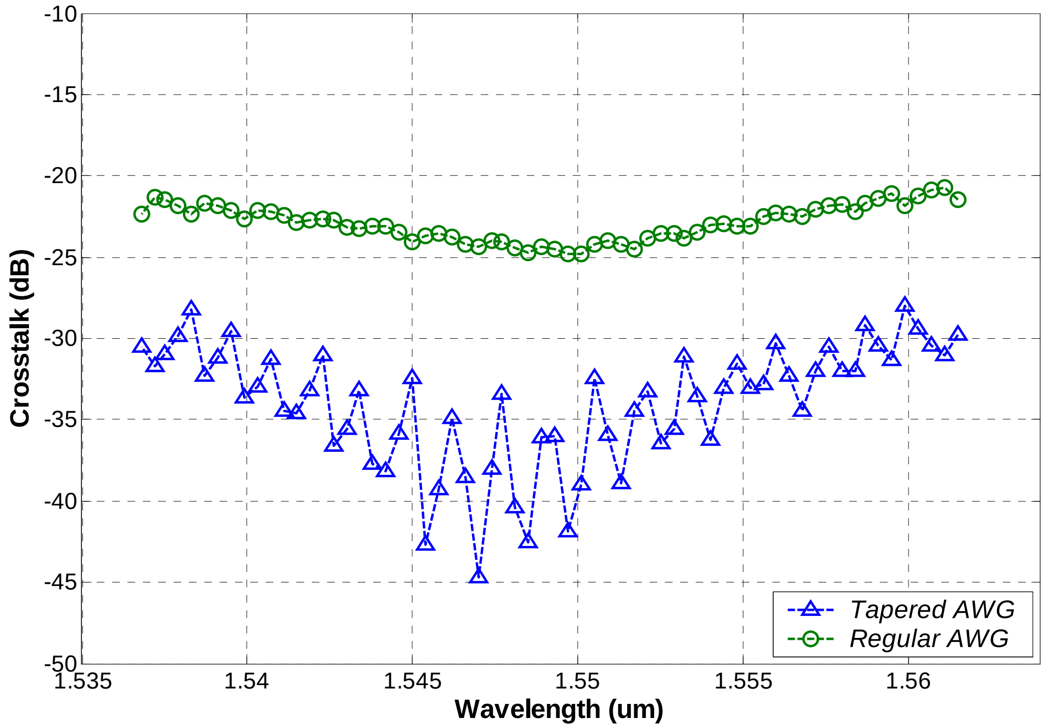

Fig. 2-15 Comparison of the crosstalk for 64×64 regular AWG and 64×64 tapered-AWG

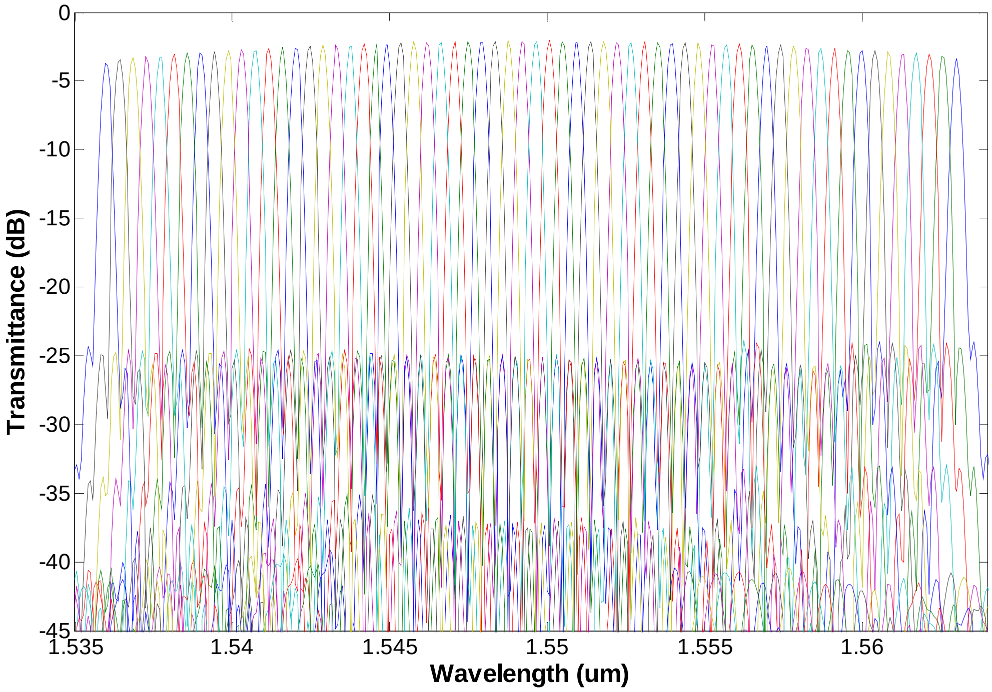

Fig. 2-16 Spectrum of 64×64 AWG with tapered waveguide

Table II Design parameters of a 64 × 64 AWG

Parameter	Symbol	Value
Number of input and output waveguide	N	64
Number of waveguide in the phase array	M	266
Free propagation length	L_{FPR}	13274.88μm
Mode field radius of the waveguide (*x=i, p ,o*, input, phase array region,	w_x	3.09
Waveguide spacing (*x=i, PA ,o*, input, phase array region, output)	d_x	7.3μm
Refractive index of Free Propagation Region	n_{FPR}	3.45
Refractive index of the phase array waveguide	n_{PA}	3.45
Group index of the phase array waveguide	n_g	3.45
Phasar order	m	22
Central Frequency	λ_c	1550 nm
Waveguide width	W	5.3μm
Shortest phase array waveguide	L_0	500μm
The length difference between adjacent phase array	ΔL	9.89μm
Free spatial range of the arrayed waveguide grating	X_{FSR}	69.56 nm
Free spectral range of the arrayed waveguide grating	FSR	8904.02 GHz

Table III High-Level requirement parameters

Parameter	Symbol	Value
Channel Spacing for Wavelength	$\Delta\lambda$	0.4 nm
Channel Spacing for frequency	Δf	50 GHz
Uniformity	L_u	1.6 dB